

FORMATION OF EARTH-LIKE PLANETS DURING AND AFTER GIANT PLANET MIGRATION

AVI M. MANDELL^{1,3,4}, SEAN N. RAYMOND² & STEINN SIGURDSSON¹

Draft version August 8, 2021

ABSTRACT

Close-in giant planets are thought to have formed in the cold outer regions of planetary systems and migrated inward, passing through the orbital parameter space occupied by the terrestrial planets in our own Solar System. We present dynamical simulations of the effects of a migrating giant planet on a disk of protoplanetary material and the subsequent evolution of the planetary system. We numerically investigate the dynamics of post-migration planetary systems over 200 million years using models with a single migrating giant planet, one migrating and one non-migrating giant planet, and excluding the effects of a gas disk. Material that is shepherded in front of the migrating giant planet by moving mean motion resonances accretes into "hot Earths", but survival of these bodies is strongly dependent on dynamical damping. Furthermore, a significant amount of material scattered outward by the giant planet survives in highly excited orbits; the orbits of these scattered bodies are then damped by gas drag and dynamical friction over the remaining accretion time. In all simulations Earth-mass planets accrete on approximately 100 Myr timescales, often with orbits in the Habitable Zone. These planets range in mass and water content, with both quantities increasing with the presence of a gas disk and decreasing with the presence of an outer giant planet. We use scaling arguments and previous results to derive a simple recipe that constrains which giant planet systems are able to form and harbor Earth-like planets in the Habitable Zone, demonstrating that roughly one third of the known planetary systems are potentially habitable.

Subject headings: astrobiology – methods: N-body simulations — planetary systems: formation

1. INTRODUCTION

More than 200 giant planets are known to orbit main-sequence stars (Butler et al. (2006); see Schneider (2006) for recent results) and all but 5 have semi-major axes within the orbit of Jupiter; more than half of known planets reside within 1 AU of their parent star. There are also a surprising number of planets at very small semi-major axes: 22% of currently known extrasolar planets have orbital radii less than 0.1 AU, and 16% are located within 0.05 AU of the central star. Limitations on the current observational techniques do not allow a complete sample of planets around solar-type stars beyond approximately 3 AU (see, e.g., Tabachnik & Tremaine (2002)), but it is clear that there is a significant population of planetary systems with giant planets at small orbital radii. The occurrence of close-in giant planets is surprising because theoretical models predict that the formation of giant planets in the hot inner regions of a protoplanetary disk would be difficult under realistic conditions (Bodenheimer et al. 2000). To explain the observations of massive planets at very small distances from their parent stars, a mechanism is necessary to move them from where they formed to where they currently reside; this process is commonly known as planetary migration (Lin et al. 1996). With the inclusion of migration of a giant planet to small orbital radii, theories on the evolution of solid bodies in the inner disk developed for our

own planetary system must be re-examined.

1.1. Giant Planet Formation and Migration

Favored theories of giant planet formation center around two main paradigms, commonly called the core accretion model and the gravitational instability model. The bottom-up core accretion model (Pollack et al. 1996; Alibert et al. 2005; Hubickyj et al. 2005) requires the accretion of planetesimals into a solid core of $\sim 5\text{--}10 M_{\oplus}$, massive enough to initiate runaway gravitational infall of a large gaseous envelope. The formation of this massive core requires a high surface density of solids, which is difficult to achieve in the hot inner disk. A jump in the surface density is believed to occur just past the "snow line", where the disk temperature drops below the freezing point of water (at ~ 170 K in protoplanetary disks (Hayashi 1981)) and ice is available as a building block. Isolation masses also increase with orbital distance r for surface density profiles flatter than r^{-2} (Lissauer 1987), also favoring formation at larger orbital distances. The top-down gravitational instability model (Boss 1998, 2000; Mayer et al. 2002; Durisen et al. 2005) assumes a gaseous protoplanetary disk massive and cold enough to become gravitationally unstable to collapse, resulting in a massive gaseous planet with little or no solid core. For realistic disk masses, this process only becomes efficient at orbital radii greater than ~ 10 AU (Mayer et al. 2002). Both are believed to be viable under certain physical conditions, but it is still unclear how each mechanism (or combination of mechanisms) functions in realistic circumstellar environments; even calculations of the core masses for the giant planets in our own system have large uncertainties (Guillot 1999; Saumon & Guillot 2004). Regardless of which mechanism forms planets in extrasolar planetary systems, it is

arXiv:astro-ph/0701048v1 2 Jan 2007

¹ Pennsylvania State University, Department of Astronomy & Astrophysics, University Park, PA 16803, USA

² NASA Postdoctoral Program Fellow, Center for Astrophysics and Space Astronomy, University of Colorado, Boulder, CO 80309-0389, USA

³ NASA Goddard Space Flight Center, Code 693, Greenbelt, MD 20771, USA

⁴ Corresponding Email: mandell@astro.psu.edu

clear that giant planets detected as small orbital radii were unlikely to form at their present locations.

A variety of potential migration mechanisms have been proposed to operate on massive planets, including planet-planet scattering (Farinella 1980; Weidenschilling & Marzari 1996; Rasio & Ford 1996), planetesimal scattering (Fernandez & Ip 1984; Murray et al. 1998), and a several types of gas-planet interactions (see Papaloizou & Terquem (2006) for a review). The most simple and robust hypothesis is known as Type II migration. Type II migration (Papaloizou & Lin 1984; Lin et al. 1996) works on planetary bodies that are massive enough to open an azimuthal and vertical gap in the gas disk, locking the planet into common orbital evolution with the gas disk. Viscosity in the gaseous disk, thought to be due primarily to the magneto-rotational instability (MRI, Gammie (1996)), results in orbital decay and infall of the gas onto the central star (as evidenced by accretion and stellar activity in young stars (Muzerolle et al. 2003; Calvet et al. 2004; Eisner et al. 2005)). Thus, the giant planet loses angular momentum and migrates inwards coupled to the gas disk. Simulations suggest Type II migration timescales range between 10^5 to a few times 10^5 years, depending on the disk and planet conditions (Nelson & Papaloizou 2004; D'Angelo et al. 2003). Planets halted at very small radii most likely ceased migration due to gas evacuation around the central star or planetary mass loss onto the central star, creating the "hot Jupiter" population (see Papaloizou & Terquem (2006) for further explanation). However, for orbital radii beyond approximately 0.1 AU these stopping mechanisms would not be effective, and other explanations are required for extrasolar planets detected in orbits between 0.1 and a few AU. The intermediate stopping distances may be a result of dissipation of the gas disk during migration (Trilling et al. 1998) or a "dead zone" where the MRI is ineffective (Gammie 1996), but these mechanisms rely on extreme fine-tuning of parameters or questionable physical conditions to explain the distribution of orbital radii for extrasolar planets.

1.2. Terrestrial Planet Formation

Standard theories of the evolution of a planetary system suggest that a circumstellar disk will proceed through various accretionary stages culminating in the final architecture of a stable planetary configuration. Coagulation of the inceptive dust particles occurs through collisional sticking until the solid bodies become massive enough to decouple from the surrounding gas disk and settle to the disk midplane, resulting in meter-sized objects on timescales of 10^4 years (Lissauer 1993; Beckwith et al. 2000). In this size range orbital decay due to gas drag is very rapid (Weidenschilling 1977) and accretion must happen very quickly to avoid infall onto the central star and overly extensive mixing. The accretion rate can be enhanced by differential migration rates (Weidenschilling 1977), gravitational instability (Goldreich & Ward 1973; Youdin & Shu 2002), and/or concentration of meter-sized bodies in spiral density waves generated in the gaseous disk (Rice et al. 2004). Once the largest bodies reach ~ 1 km in size, their gravitational cross-section becomes larger than their ge-

ometric cross-section and they begin the phase known as "runaway growth". During this phase the largest bodies grow faster than the smaller bodies due to gravitational focusing and damping due to dynamical friction, resulting in a widening mass dispersion (Greenberg et al. 1978; Wetherill & Stewart 1989; Weidenschilling et al. 1997). "Runaway growth" transitions into "oligarchic growth" when the velocity dispersion of planetesimals becomes comparable to the escape speed of the largest embryos (Kokubo & Ida 1998), stalling accretion for the largest bodies and decreasing the embryo mass dispersion. Oligarchic growth ends after approximately 10^{6-7} years when the oligarchs have depleted their "feeding zones" sufficiently such that dynamical friction is no longer effective, and embryos begin to scatter each other (Kokubo & Ida 1998, 2000). The final "chaotic phase" of planet growth proceeds through scattering and collisions between the large protoplanets and final clearing of the remaining planetesimals to produce a stable planetary system after more than 10^8 years (Wetherill 1996; Chambers 2001; Raymond et al. 2006c; Kenyon & Bromley 2006).

Though the evolutionary state of the protoplanetary disk at the inception of giant planet migration is uncertain, there are several reasons to believe that relatively large objects would exist in the inner disk by the time migration begins. Recent giant planet formation models assuming core accretion as the dominant mechanism give full formation timescales ranging from 5 Myr to less than 1 Myr (Rice & Armitage 2003; Alibert et al. 2005; Hubickyj et al. 2005), corresponding to the oligarchic growth stage in standard terrestrial planet models. Observations of gas and dust in primordial disks give disk lifetimes of $\sim 10^7$ years for gas (Briceno et al. 2001; Haisch et al. 2001) and less than 3 Myr for dust (Silverstone et al. 2006), suggesting that solid bodies form long before the gas disk dissipates. For our own Solar System, radioactive dating of meteorites give equivalent ages for both the earliest chondrule formation and differentiation in asteroidal bodies in our own Solar System, supporting rapid evolution of large solid bodies (Kleine et al. 2002). Timescales for giant planet formation by gas instability may be as short as 10^3 years, but in the massive disks required for gas instability to function the migration mechanisms may be halted until much of the gas has dissipated (Boss 2005). Likewise, if massive disks are indeed required for giant planets to form quickly enough for migration to occur, formation timescales in other parts of the disk as would most likely be shortened as well.

One of the most interesting problems in the formation of planetary systems is the distribution of volatiles compared with refractory materials in different planetary bodies. Naturally, the final composition of planets formed through the scenario described above depends on both the initial distribution of material in the protoplanetary nebula and the subsequent dynamical evolution of the system. The initial composition of solids in a circumstellar disk is expected to follow a basic condensation sequence (Grossman 1972), but the effects of radial transport of grains and mm to meter-sized objects through turbulence or radial drift have the potential to dramatically re-arrange this early compositional gradient

(Stevenson & Lunine 1988; Stepinski & Valageas 1997; Ciesla & Cuzzi 2006). However, evidence from our own system suggests that late-stage protoplanetary material may maintain the gross characteristics of the basic condensation sequence: analysis of chondrites in meteorites from parent bodies in different regions of the inner solar system suggest a constant increase from almost no water at 1 AU to almost 10% water at 2.5 AU (Abe et al. 2000), with cometary bodies thought to contain at least half of their mass in water ice. The dry nature of asteroidal material in the vicinity of Earth further suggests that continued delivery of water-rich material must have been necessary to produce the current water inventory, either through comet impacts (Owen & Bar-Nun 1995) or through accretion of disrupted asteroidal material (Morbidelli et al. 2000). The importance of radial transport of material in defining the final composition of terrestrial planets has been confirmed by N-body simulations, which suggest that late-stage accretion of water-rich material is largely influenced by the characteristics of giant planets in these systems, notably their orbital eccentricities (Chambers & Cassen 2002; Raymond et al. 2004; Raymond 2006).

1.3. Previous Work

With the uncertainty inherent in the cornucopia of forces that may be functioning on objects in various different size regimes in circumstellar disks, untangling the complex dynamics during the formation and evolution of solid bodies in the inner regions of a protoplanetary disk becomes difficult. Several studies concerning the habitability of planetary systems in a variety of conditions made the simple assumption that systems with close-in giant planets could not be habitable (Lineweaver 2001; Gonzalez et al. 2001). Given the 'hot Jupiter'-stellar metallicity correlation (e.g., Fischer & Valenti (2005)), this placed limits on the galactic locales likely to harbor Earth-like planets (the so-called 'Galactic Habitable Zone'; Lineweaver et al. (2004)). More recent studies have concentrated on exploring the dynamical effects of giant planet migration on a simplified disk, with varying results. Armitage (2003), assuming planetesimals in the inner disk would be destroyed by a migrating giant planet, analyzed the evolution of the post-migration disk surface density with a simple dust coagulation formulation. They found that if migration begins after significant embryo formation has occurred, post-migration formation would be unlikely due to dust depletion and insufficient remaining material. In Mandell & Sigurdsson (2003) we examined the assumption of planetesimal destruction during migration by analyzing the probability of terrestrial-mass objects surviving the inward migration of a giant planet. We used dynamical modeling to investigate the survival rate and the eccentricity and semi-major axis distribution of objects using different initial orbital radii and different giant planet migration rates, and concluded that up to 50% of objects could remain in the system, albeit with a large eccentricity distribution. Edgar & Artymowicz (2004) also examined the dynamical impact of the migration of a planet of various sizes on a planetesimal disk, concluding that eccentricities could rise as high as 0.4 but would be damped down quickly in the presence of gas.

Several studies have recently begun to investigate the

evolution of a more realistic protoplanetary disk, both during migration and in a post-migration configuration. Fogg & Nelson (2005) and Fogg & Nelson (2006) analyzed the survival rate of inner-disk objects during migration in a range of size regimes approximating runaway growth, including the effects of gas drag and subsequently a more realistic evolving disk model. They concluded that between 50 and 90% of material would be retained, with the distribution interior and exterior to the giant planet varying with disk maturity. Alternately, Raymond et al. (2005) examined the formation and composition of terrestrial planets in the presence of an existing inner giant planet at varying stopping distances and without a gas disk, concluding that a hot Jupiter would have little influence on terrestrial planet formation outside its orbit. That study proposed that terrestrial planet formation would be inhibited for orbits with periods within a factor of 3 - 4 of either an outer or inner giant planet.

In this study we present detailed analysis of numerical simulations in which we explore the final stages of terrestrial planet formation after the migration of a giant planet. Simulations begin with a two-phase protoplanetary disk and a fully-formed giant planet in the outer disk, and follow the system through the giant planet's migration and 200 Myr of additional evolution, sufficient to examine the final characteristics of planets in the terrestrial zone. These results bridge the gap between the short-term effects of migration on the planetesimal disk demonstrated by Fogg & Nelson (2005) and the long-term evolution and final configurations of planetary systems with close-in giant planets explored by Raymond et al. (2005). A subset of these simulations were first presented in Raymond et al. (2006b) (referred to here as Paper I), and in this paper we present two additional simulation sets run with different initial conditions and a detailed description and analysis of all three simulation sets.

In Section 2 we describe the simulation details and initial conditions; in Section 3 we describe the results for all the simulations and compare the three different models; in Section 4 we explore the potential ramifications for known extrasolar planetary systems; and in Section 5 we provide a summary of our results and suggest future work.

2. MODEL PARAMETERS

2.1. Initial Conditions

We performed three different sets of simulations to examine the effects of the most important parameters in the simulations: the number and location of giant planets and the presence of a gaseous disk during and after migration. The primary set includes only one Jupiter-mass planet that migrates, and includes the viscous damping effects of a gaseous disk. The second set has both a migrating Jupiter-mass planet and a Saturn-mass planet stationary at 9.5 AU, with viscous damping included. The final set includes the two giant planets but does not incorporate gas drag. Our three sets of simulations are named JD for 'Jupiter and (gas) Drag', JSD for 'Jupiter, Saturn and Drag', and JSN for 'Jupiter, Saturn, No drag'. Using different random number seeds, we generated five disks of randomly distributed embryos and

planetesimals for each set. However, one run in each simulation set was unusable due to corruption in the data storage or transfers between processors; therefore final results are presented here for four simulations in each set, resulting in a total of twelve simulation results. The first four simulations (JD) were presented in Paper I; we incorporate them here as part of the larger set of simulations.

The disk models used in this study have three major components: a solid disk of small protoplanetary bodies, a gaseous disk, and one or two fully-formed giant planets. We start our simulations at the end of the oligarchic growth phase of the protoplanetary disk, such that ~ 1000 -km planetary embryos have formed throughout the disk but the mass in km-sized planetesimals is comparable to the mass in embryos (Kokubo & Ida 1998, 2000). Additionally, we incorporate the dissipative damping from a decaying gas disk, which disappears after 10 Myr (Briceño et al. 2001; Haisch et al. 2001). Finally, we include either one or two giant planets, assuming them to be fully-formed by this stage due to rapid formation processes in the outer disk. This is consistent with recent results showing that giant planets may form in < 1 Myr via either core-accretion (Rice & Armitage 2003; Alibert et al. 2005; Hubickyj et al. 2005) or gravitational collapse (Boss 2001; Mayer et al. 2002, 2004).

The radial surface density profile of the solid material in the disk follows from the minimum-mass solar nebula model (MMSN; Weidenschilling (1977); Hayashi (1981)):

$$\Sigma(r) = \Sigma_1 f \left(\frac{r}{1\text{AU}} \right)^{-3/2} \quad (1)$$

where Σ_1 is the surface density at 1 AU in an MMSN disk ($\sim 6 \text{ g/cm}^2$ and 1700 g/cm^2 for the solid and gaseous components, respectively; Hayashi (1981)) and f is a scaling factor for the total surface density. Since the presence of close-in giant planets correlates with stellar metallicity (e.g. Laws et al. (2003)), we model a significantly more massive disk than the MMSN, with $f \approx 2.2$. Similarly, the nebular gas density follows an exponential profile of the form

$$\rho(r, z) = \rho_0(r) \exp \left\{ -z^2/z_0(r)^2 \right\} \text{ g/cm}^3 \quad (2)$$

as described by Thommes et al. (2003), where ρ_0 is the midplane density taken from the MMSN:

$$\rho_0^{\text{min}}(r) = 1.4 \times 10^{-9} (r/1 \text{ AU})^{-11/4} \text{ g/cm}^3 \quad (3)$$

and z_0 is disk vertical scale height given by

$$z_0(r) = 0.0472 (r/1 \text{ AU})^{5/4} \text{ AU} \quad (4)$$

The gas density decreases linearly over 10 Myr, simulating the removal of the gaseous nebula on observed timescales (Briceño et al. 2001; Haisch et al. 2001).

Figure 1 illustrates our initial conditions for a single run. The initial solid disk is composed of ~ 80 planetary embryos and 1200 planetesimals. It extends from 0.25 to 4.5 AU (with a ~ 2 Hill radii gap on either side of the Jupiter-mass planet at 5.2 AU), and then from 6 AU to 9 AU. The solid disk comprises $17 M_\oplus$, of which $10 M_\oplus$ is equally distributed between planetesimals and embryos from 0.25 to 4.5 AU. Embryos between 0.25 and 4.5 AU

are spaced randomly by $\Delta=5$ -10 mutual Hill radii, and have masses between roughly 0.01 and $0.4 M_\oplus$ with a mean of $0.11 M_\oplus$. Embryo masses M_{emb} increase with radial distance r as $M_{\text{emb}} \propto \Delta^{3/2} r^{3/4}$ (Raymond et al. 2004). In the inner region between 0.25 and 4.5 AU are 1000 planetesimals of $0.005 M_\oplus$ each, distributed radially as $r^{-1/2}$, i.e. as the annular mass in our surface density distribution. The surface density distribution has a jump immediately past the snow line, assumed to lie at 5 AU; therefore, isolation masses are larger in the region from 6 to 9 AU. In this outer region we space embryos by $\Delta=3$ -6 mutual Hill radii, forming only 4 - 7 embryos between 0.2 and $1.1 M_\oplus$, with a mean of $0.6 M_\oplus$ and totaling $5.7 M_\oplus$. In addition, 200 planetesimals comprising $1.3 M_\oplus$ are placed in the region. The higher embryo mass - planetesimal mass ratio in the outer region reflects the faster embryo formation time in this higher density region. Indeed, massive embryos *must* have formed quickly in this scenario (if giant planets form via core-accretion), because the giant planets are already fully-formed. Starting eccentricities are randomly selected up to 0.02 and inclinations are set at 0.1° , but these initial values are inconsequential since the distributions are quickly perturbed.

Each embryo and planetesimal is assigned a composition based on its starting location. Water and iron contents are based on values from our Solar System, where comets are thought to contain almost half their mass in water ice and asteroids beyond ~ 2.5 AU contain significant quantities of water (Abe et al. (2000); see Section 1.2 and Fig. 2 from Raymond et al. (2004)). Inside 2 AU, embryos and protoplanets are assumed to be dry, and beyond 5 AU they contain 50% of their mass in water. Between 5 AU and 2.5 AU they contain 5% water by mass, and from 2-2.5 AU they contain 0.1% water by mass; this distribution corresponds to starting mean water mass fraction of $\sim 8 \times 10^{-3}$ inside 5 AU (see Figure 1). Starting iron contents are interpolated between the known values of the planets (values from Lodders & Fegley (1998)), including a dummy value of 0.4 in place of Mercury because of its anomalously large iron content (Raymond et al. 2004, 2005); the starting mean iron mass fraction is ~ 0.32 inside 4.5 AU and ~ 0.13 beyond 6 AU.

Embryos and giant planets interact gravitationally with every body in the system. Planetesimals, however, are non self-interacting and are given an effective mass to simulate a collection of much smaller particles (e.g. Thommes et al. (2003)). In this way we can realistically include the effects of 1) gas drag on planetesimals and 2) dynamical friction of planetesimals on embryos while using a reasonable particle number. Collisions are treated as inelastic mergers conserving water and iron (for a discussion, see Raymond et al. (2004)).

2.2. Simulation Details

Numerical simulations were performed using a modified version of the publicly-available hybrid symplectic integrator package MERCURY by Chambers & Migliorini (Chambers & Migliorini 1997; Chambers 1999). We integrated each simulation for 200 Myr with a 2-day timestep, which accurately integrates orbits with apocenter distances larger than roughly 0.05

AU (Levison & Duncan 2000). Energy is not properly conserved for orbits inside 0.05 AU – these bodies are typically given an artificial energy “kick” that results in a close encounter and dynamical ejection. This effect is important in certain instances and is discussed further in Section 3.5.

To examine the effects of migration, we modified the integrator to accommodate an artificial inward migration of a giant planet, as discussed in Mandell & Sigurdsson (2003). We use a simple drag force as described in Chiang et al. (2002) that produces a linear inward migration:

$$\mathbf{F}_{mig} = \frac{-M_P \mathbf{v}_P}{t_{mig}} \quad (5)$$

where M_P and \mathbf{v}_P relate to the planet and t_{mig} is the migration time. This method for simulating migration produces no artificial changes in eccentricity and inclination for the migrating planet, and therefore removes the potential for non-physical orbital excitation of the giant planet. Migration rates as a function of time were modeled after recent simulations of Type II giant planet migration in the literature, which range from 10^5 to 10^6 years (D’Angelo et al. 2003; Nelson & Papaloizou 2004) with an exponential tail to simulate potential braking processes (see Sect 1).

In addition, a basic fluid drag force was instituted to simulate the dissipation of energy due to the surrounding gaseous disk. The gas drag takes the basic form of Stokes drag:

$$\mathbf{a}_{drag} = -K v_{rel} \mathbf{v}_{rel} \quad (6)$$

where v_{rel} is the relative velocity of the object with respect to the surrounding gas. The drag parameter is defined as

$$K = \frac{3\rho_{gas}C_D}{8\rho_m r_m} \quad (7)$$

where ρ_{gas} refers to the local gas density, ρ_m and r_m refer to the density and mass of the object and the drag coefficient C_D is defined to be 1 (Adachi et al. 1976). The gas disk is assumed to revolve in a circular orbit at sub-Keplerian velocity due to internal pressure support, following the relation

$$v_{gas} = v_K(1 - \eta) \quad (8)$$

with η defined as

$$\eta = \frac{\pi}{16}(\alpha + \beta) \left(\frac{z_0(r)}{r} \right)^2 \quad (9)$$

where α and β are the exponents of radial dependencies of density and temperature respectively and z_0 is the radially-dependent vertical disk scale height, defined below (Thommes et al. 2003). The solid bodies therefore experience both a orbital damping effect and an inward migration, decreasing with mass and increasing with gas density.

In these simulations we do not account for torques on sub-Saturnian sized bodies due to density waves in the gas disk, which may lead to a reduced velocity dispersion (known as gravitational or tidal gas drag; Ward

(1993)) and/or orbital decay (known as Type I migration; Ward (1997)) of embryo and planet-sized bodies. We neglect these effects primarily because the role of disk torques on fully-embedded objects is still uncertain. Type I migration rates from simulations range from 10^3 to 10^6 years (Tanaka et al. 2002; D’Angelo et al. 2003), which would alternately result in either the loss of all solid bodies before the gas disk has disappeared, or very little change in orbital position for large bodies. It is even unclear whether migration or damping due to disk torques functions at all in realistic turbulent gas disks (Nelson & Papaloizou 2004; Laughlin et al. 2004). McNeil et al. (2005) investigated the oligarchic stage of terrestrial planet formation for different Type I migration scenarios, demonstrating that faster migration rates serve to damp down excitation and widen embryo spacing for material within ~ 2 AU. This may prove to be important in determining the final mass and composition of terrestrial planets, but since the rate of migration of protoplanets compared with the migrating giant planet has a significant impact on the scattering energy and angular momentum transfer between the giant planets and the surrounding solid bodies, arbitrarily choosing a migration rate would strongly influence the results. We therefore chose not to include it in this work. Future simulations will incorporate more detailed models of embryo migration taken from improved hydrodynamic simulations.

3. RESULTS

The evolution of the protoplanetary disk can be separated into distinct dynamical stages. Migration (Stage 1) encompasses the migration period, during which the giant planet moves through the interior regions of the disk. Gas Dissipation (Stage 2) begins after giant-planet migration has ceased, and continues until the remaining gas disk has fully dissipated. Clearing (Stage 3) includes the final stages of accretion and clearing in the absence of any gaseous material. In the following subsections we describe each stage, and illustrate the differences between the results for the three different models used in our simulations. Snapshots during the different stages of the evolution of each type of simulation are illustrated in Figures 2 (JD), 3 (JSD), and 4 (JSN). Each plot follows the evolution of all bodies in the simulation, and tracks their masses, orbital parameters and compositions through time. In addition, the mean and range of orbital and compositional properties for each model at the end of each stage are listed in Tables 1, 2, and 3.

3.1. Stage 1: Migration

During Stage 1 the Jupiter-mass planet migrates inwards from 5.2 to 0.25 AU over 10^5 years, and the inward progression of mean motion resonances results in the shepherding and orbital excitation of the disk material interior and exterior to the giant planet. As the Jupiter-mass planet continues through the inner disk, material is either scattered outward or captured into resonant orbits and forced to migrate inward with the Jupiter-mass planet. This resonance capture, noted by Tanaka & Ida (1999), occurs when a body close to a strong mean motion resonance (e.g., the 2:1 MMR) has its orbit excited and its eccentricity increased. Thus, the body’s periheli-

lion distance has decreased and it has lost angular momentum. An eccentric orbit increases the relative velocity between the protoplanet and the pressure-supported gas disk, thereby increasing the effects of gas drag. In addition, an eccentric orbit encounters more nearby planetesimals and also enhances dynamical friction. These dissipative forces tend to reduce the body’s energy and decrease its semi-major axis and eccentricity. Thus, the protoplanet is moved inward of the resonance with the giant planet; as the giant planet continues to migrate, the resonance can continue pushing it inward due to these angular momentum loss mechanisms. Smaller bodies that feel gas drag more strongly can be pushed inward by higher-order resonances. This is clearly seen in Fig. 2, where protoplanets are pushed inward by the 2:1 and 3:2 resonances, and planetesimals by the 8:1 resonance. The decreasing spacing between resonances enhances the accretion and scattering rate as the giant planet moves inward, with planetesimal encounters peaking at approximately 7×10^4 years when the Jupiter-mass planet’s semi-major axis reaches ~ 0.4 AU and the 2:1 resonance reaches the inner edge of the disk (see Figure 6). At the end of the giant planet’s inward migration, the remaining disk material is divided between bodies captured in very close low eccentricity orbits in interior resonances with the Jupiter-mass planet and bodies in high eccentricity orbits beyond 0.5 AU.

In the simulations including the presence of a gas disk (Models JD and JSD) orbital excitation of planetesimals is almost completely damped in the inner disk - by the end of Stage 1 the mean eccentricity for planetesimals within 9.5 AU is less than 0.1, compared with approximately 0.5 for embryos; mean inclination follows similar trends but with slightly higher values for bodies in the JSD simulations due to multiple scatterings (see Table 1). The excitation of embryos is damped by a combination of relatively weak gas drag and dynamical friction from interactions with planetesimals. These effects are sufficiently strong to halt almost all ejections, and the orbital radii of scattered bodies are limited to within 50 AU. Additionally, these forces result in strong resonant trapping by the migrating planet, frequent collisions and a rapid increase in embryo masses - Figure 7 reveals that the large majority of both embryo-embryo collisions and embryo-planetesimal collisions occur during the migration period, and Figure 5 demonstrates the loss of planetesimal mass to embryo mass. By the time migration has ended, the combination of rapid accretion and scattering has cleared almost all planetesimals from within 5 AU, and the average embryo mass for this region has risen from $0.11 M_{\oplus}$ in ~ 65 objects to $0.45 M_{\oplus}$ in ~ 17 objects. Eccentricities for remaining embryos beyond 0.5 AU are evenly distributed from 0.2 to 0.8, increasing with semi-major axis (see Figures 2 and 3); this relationship is characteristic of a scattered population of embryos as noted by Mandell & Sigurdsson (2003). Inclinations remain low due to damping, with average inclinations remaining below 5° (see Table 1). Within 5 AU the mean composition of embryos does not change drastically since the bodies surviving in the inner disk are not augmented by any additional material over these short timescales, but the material is locally mixed. The exception is the JSD model, where water-rich material is scattered inward by the outer Saturn-mass planet and the mean water

mass fraction increases by a factor of 2.

Beyond 5 AU the dynamical effects of the presence of a second giant planet become important. In simulations without a second planet, the only external excitation for objects orbiting beyond the initial orbit of the migrating Jupiter-mass planet comes from external resonance crossings and mutual gravitational interactions. Material native to this region remains relatively undisturbed, with very little orbital excitation. Bodies scattered into the region by the migrating giant have large eccentricities that are subsequently damped on Myr timescales. Maximum orbital eccentricity for these outer embryos increases up to ~ 0.5 , and by the end of migration dynamical friction and damping due to gas drag reduce the maximum eccentricity to ~ 0.2 (see Figure 2). In the JSD simulations, small bodies in the outer system are excited by both mean motion resonances and gravitational scattering. This results in a significant scattered planetesimal population beyond 9.5 AU with a mean eccentricity of 0.3 and inclinations up to 30° . A small number of embryos are also scattered by both the migrating Jupiter-mass planet and the outer Saturn-mass planet, resulting in a semi-major axes as high as 50 AU.

In addition to the presence of material remaining outside the orbit of the close-in giant planet, all simulations including gas drag form one or more terrestrial-mass bodies residing within the orbit of the Jupiter-mass planet (see Figure 10). These small bodies are the result of resonant shepherding by the giant planet as it migrates inward, and accretion at the resonance can build up bodies of several M_{\oplus} . These “Hot Earths” are analogous to the $7.5 M_{\oplus}$ planet found by radial velocity searches around the M star GJ 876 (Rivera et al. 2005) and suggest that this phenomenon is common. Other computational studies have demonstrated resonant shepherding as a mechanism to explain hot Earths (Zhou et al. 2005; Fogg & Nelson 2005, 2006), though Zhou et al. (2005) explain the planet around GJ 876 by invoking moving secular resonances during disk dissipation rather than mean-motion resonances during migration. However, in almost all of the simulations the inner ‘hot Earth’ becomes unstable as the gas disk disappears and either impacts the Jupiter-mass planet or is ejected. Similarly, in simulations without any gas drag almost no accretion occurs interior to the migrating giant planet. This sensitivity to damping forces was noted by Fogg & Nelson (2006), but may be mitigated by the presence of collisional debris not included in these simulations. More detailed work is necessary to accurately model the long term stability of these bodies.

Simulations performed without the presence of a gas disk (Model JSN) demonstrated very different encounters between bodies than Models JD and JSD throughout the disk. Without the damping effects of gas drag on planetesimals, accretion ceases after $\sim 40,000$ years as the Jupiter-mass planet enters the inner system (see Figure 7). Excitation from resonance crossings and direct scattering cause $\sim 40\%$ of the mass in small bodies to be lost from the system by the end of migration (see Figure 5 and Figure 6), with the remainder of material distributed evenly in eccentricity and inclination phase space. Approximately 65% of the remaining mass still resides within 10 AU (compared to 75% for simulations with gas drag), but the ratio of the total mass in embryos

to the total mass in planetesimals in this region has only risen to only ~ 2 , compared to ~ 10 for simulations including the effects of a gaseous disk. The mean embryo mass is $0.18 M_{\oplus}$ compared with $0.45 M_{\oplus}$ for the simulations with gas drag, and the mean eccentricity and inclination for both embryos and planetesimals are both significantly higher than the JD and JSD simulations.

3.2. Stage 2: Gas Dissipation

Once the Jupiter-mass planet has ceased migrating at 0.25 AU, the remaining bodies in the disk continue to scatter and accrete each other during Stages 2 and 3, similar to the classical oligarchic and chaotic stages of terrestrial planet formation. At the start of Stage 2 the protoplanetary embryos in the disk are dynamically hot, with mean eccentricities increasing with orbital radius. However, during Stage 2 the presence of gas drag and dynamical friction serve to damp down eccentricities and inclinations and replenish the inner disk due to migration of planetesimals. During this stage the location and rate of accretion depends critically on the balance between the size of planetesimals and embryos and the density of the gas disk: faster migration leads to higher accretion rates at smaller orbital radii, while damping of dynamical excitation leads to reduced accretion and resonance capture.

After a hiatus of several million years due to clearing by the giant planet migration and damping by the remaining gas disk, the accretion of planetesimals increases over the final duration of Stage 2 as a result of the refilling of feeding zones due to planetesimal orbital decay and increased orbital crossing due to decreased gas drag (see Figure 7 for the accretion history of the combined data sets). The accretion wavefront proceeds inward as the gas becomes less dense and orbital excitation increases. This late-stage accretion is responsible for the high water mass fractions seen in the final configurations - embryos acquire most of their mass during Stage 1, but most of their water during Stage 2 (see Figure 9). In simulations with the JD model accretion continues until after the gas has disappeared, but the presence of a second massive planet in the JSD model leads to clearing between 5 - 15 AU and a decrease in accretion after 5×10^6 years. The outer planet also serves to clear out high-eccentricity embryos, leading to a much lower mean eccentricity and fewer embryos in the outer disk as compared with the JD model (see Table 2). After 10 Myr the mass in planetesimals in both the JD and JSD models is only $\sim 1 M_{\oplus}$, but the total mass in the JSD simulations is less than 30% of the mass remaining in the JD simulations due to embryo ejection in the outer system (see Figure 5, Table 2). Eccentricities and inclinations in the inner system for both models decrease dramatically over the lifetime of the gas disk, with embryo eccentricities and inclinations decreasing by 20-50% and planetesimals attaining a mean eccentricity below 0.1 and a mean inclination less than 2° .

3.3. Stage 3: Clearing

In the simulations with gas drag, Stage 3 begins as the final gas disk dissipates and dynamical interactions begin to excite the remaining solid bodies. Accretion rates decrease steadily and cease by approximately 30 Myr,

and scattering and ejection clear out most of the material in the inner disk over the remaining 170 Myr (see Figure 6). At the end of the simulations only a few large protoplanets are left in the inner disk, but longer dynamical timescales in the outer disk result in longer clearing times and increased final eccentricities and inclinations for the JD simulations - the mean eccentricity rises to ~ 0.3 and inclinations increase up to $\sim 50^{\circ}$ (see Table 3). In contrast, the Saturn-mass planet begins to excite and scatter bodies near the end of Stage 2, and continues to eliminate highly excited bodies so that the mean eccentricities and inclinations for embryos at the end of 200 Myr are below 0.2 and 20° respectively. The few remaining planetesimals are scattered randomly in eccentricity and inclination space.

In the JSN simulations, the system moves directly from Stage 1 to Stage 3. Ejections of both embryos and planetesimals increase over the first 10 Myr, then begin to tail off (see Figure 6). Eccentricities maintain a flat distribution up to 0.7 due to a random distribution of scattering energies, while inclinations are spread out to 60° . More than 70% of the total mass is lost by 5 Myr due to ejection and impacts with the central star, leaving only a small number of embryos in chaotic orbits and a scattered population of planetesimals (see Figure 4). By 10 Myr the total mass in embryos is only 3 times the mass in planetesimals, compared with a total embryo/planetesimal mass ratio greater than 10 for the simulations with gas drag included. Highly excited bodies are cleared out of the inner system over the remainder of the simulation period and the mean eccentricity and inclination of the remaining embryos decrease to 0.25 and 17° respectively, but the planetesimals remain in highly inclined and eccentric orbits.

3.4. Final Configurations

Figure 11 shows the final configurations of all twelve of our simulations, with the Solar System included for comparison. The details of the final planetary properties for bodies within 5 AU are listed in Tables 4, 5 and 6. As seen in previous simulations (e.g., Chambers (2001); Raymond et al. (2004)), a diversity of outcomes exists within each group of similar simulations.

Clear differences can be seen between the different sets of simulations, in particular between simulations with (JD and JSD) and without (JSN) gas drag. Both the mean planet mass and the mean water mass fraction in simulations with drag is much higher than without drag. These trends have two root causes: 1) the survival of bodies scattered during migration depends strongly on drag as a dissipative force, leaving more material in the system when gas is present and promoting radial mixing, and 2) icy planetesimals from beyond 5 AU can spiral in to the terrestrial zone over the lifetime of the gas disk. Simulations with drag also form large hot Earths due to resonance capture by orbital damping (discussed in Section 3.1); Figure 10 demonstrates that all the hot Earths lie just inside resonances with the hot Jupiter. These hot Earths are rare in simulations without drag - only simulation JSN-3 formed a dry, $0.22 M_{\oplus}$ hot Earth at 0.05 AU. We attribute the existence of this planet to damping from dynamical friction during migration rather than gas drag, but scattering and ejection is much more likely under these circumstances and the probability of a

massive body surviving is low. Also, the final radius of the close-in giant planets' orbits are scattered in the gas drag simulations, due to the artificial migration caused by non-physical giant planet - planetesimal effects (discussed in Section 3.5); in simulations without drag the giant planet remains at 0.25 AU.

There also exist differences between simulations with and without an outer giant planet. The JD simulations contain extensive scattered disks beyond a few AU with high inclinations and eccentricities and very long accretion timescales, reminiscent of the Solar System's scattered disk of comets beyond Neptune (Luu et al. 1997; Duncan & Levison 1997). These disks are likely to produce vast amounts of cold dust and may be detectable around other stars; late-stage accretion and fragmentation due to this scenario could be responsible for the debris disks seen around intermediate-age main-sequence stars such as β Pictoris (Golimowski et al. 2006; Bryden et al. 2006). Outer disk material is cleared out in simulations with an outer giant planet, greatly reducing the amount of surviving outer disk material, suggesting that dust mass production could correlate positively with giant planet migration and negatively with giant planet survival in the outer system.

Potentially habitable planets survive in almost all of the simulations. In the eight simulations with drag, seven planets larger than $0.2 M_{\oplus}$ (including two in simulation JSD-4) formed in the Habitable Zone, the orbital region where the stellar flux is sufficient to maintain liquid water on the surface of a planet (assumed to lie between 0.8 and 1.5 AU for these simulations; Kasting et al. (1993)). Five planets with masses from 0.13 to $0.4 M_{\oplus}$ formed in the Habitable Zone in the four simulations without drag. In two separate cases, however, two planets remain in the Habitable Zone on crossing orbits (sims. JSN-2 and JSN-5). In each case both of the planets have inclinations of $\sim 20^{\circ}$ so the timescale for the two planets to collide is long. Long-term dynamical studies are necessary to confirm the stability of these planets on billion-year timescales. Planets as large as $1 M_{\oplus}$ form within 5 AU in simulations without gas drag, but it seems clear that additional material (either through a more massive disk or an inward flux) is necessary to form similarly sized planets in the Habitable Zone.

3.5. Drag-Induced Inward Migration

In some cases, the inner gas giant and/or surviving embryos underwent additional migration during the course of Stage 2. The cause of this additional migration originates with the resonance capture of planetesimals spiraling inward due to gas drag. In most cases, the planetesimals become trapped in outer resonances, then cascade down to just outside the 2:1 mean motion resonance with the giant planet. This outer resonance capture was investigated by Thommes (2005) with regard to larger objects, focusing on differential migration due to differences in Type II (giant planet) and Type I (terrestrial planet) migration rates. In this case, the inward migration comes from aerodynamic drag, and the capture process is aided by damping of eccentricities by the gas disk. The effect is strongest in the inner disk where gas densities are high, and once the gas disk dissipates the planetesimals are excited and either accreted onto the larger object or ejected from the system.

The combination of angular momentum loss from the larger object to the planetesimals (through orbital excitation from the strong resonance interaction) and transfer of this angular momentum from the planetesimals to the gas disk (in the form of orbital damping) leads to a net loss of angular momentum from the solid bodies and subsequent orbital decay. The amount of inward migration varied from simulation to simulation, depending on the orbital radius and number of planetesimals trapped in resonance. The total amount of inward movement of giant planets ranged from zero to almost 0.2 AU – in most cases it was about 0.1 AU. For terrestrial embryos at 1 AU the inward migration was similar, but no additional inward motion was apparent for objects beyond 1.5 AU (see Figure 8 for examples). The effect on the final orbits of the terrestrial bodies was usually overshadowed by orbital rearrangement due to late impacts and scattering events. The additional inward motion of the inner Jupiter-mass planet also caused the orbits of close-in terrestrial planets in some simulations to become too small to be properly resolved with our 2 day timestep (Levison & Duncan (2000)). These orbits became unstable and usually collided with the close-in giant planet.

Though this additional source of inward migration represents an interesting avenue for future work, the effect cannot be properly analyzed in this study due to our unusual treatment of the physical qualities of the planetesimals. As noted in Section 2.2, the planetesimals have a dynamical mass of a body with a size of ~ 1000 km, but interact with the gas disk with a more realistic cross section of a collection of 10 km bodies. Thus, the rate of angular momentum transfer for a single planetesimal caught in resonance is equivalent to that of 10^6 smaller bodies. Additionally, for computational efficiency planetesimals do not self-interact. Thus, when trapped in the same resonant orbit these small bodies are unable to coagulate into a larger body that would lose angular momentum to the gas disk less efficiently. The angular momentum loss and subsequent orbital decay over the duration of the gas disk is therefore much greater than would be present in a realistic system.

3.6. Water Delivery

Water-rich material is accumulated by the growing planets throughout their accretion. As shown in Paper 1, two primary mechanisms contribute: 1) radial mixing induced by large eccentricities as a result of scattering interactions with the migrating giant planet; and 2) accretion of in-spiraling icy material because of gas drag. The first mechanism delivers water mainly in the form of hydrated asteroidal material and takes place through each stage, although the vast majority of radial mixing occurs through giant planet scattering during Stage 1, with additional embryo-planetesimal scattering occurring during Stage 3 after the gas disk has dissipated. This mode of transport is similar to the model of Morbidelli et al. (2000), except that it is substantially enhanced by the large eccentricities induced by close encounters between the migrating giant planet and the smaller bodies. The second mechanism occurs mostly during Stage 2 as water-rich material filters through the inner system over long timescales. In our own system this mechanism most likely contributed little if any water to the Earth because of Jupiter's presence: in-spiraling icy

bodies would have first encountered Jupiter and been scattered outward or accreted. In the simulations presented here, the very water-rich planetesimals originating past 5 AU move inward quickly, but damping of excitation diminishes collisions with embryos and allows the small bodies to reach sub-AU radii. Accretion of these bodies tends to occur shortly after gas dissipation when damping ceases and their eccentricities and inclinations are increased by perturbation from nearby terrestrial bodies, resulting in collisional orbits.

As discussed in Paper 1 and below, the water contents of Habitable Zone planets in the simulations with gas drag are very high, with typical values of $\sim 10\%$ water by mass. However, it is difficult to translate these into likely values, since we do not take water depletion from impacts (Genda & Abe 2005; Canup & Pierazzo 2006) or hydrodynamic escape (Matsui & Abe 1986) into account. Previous simulations with a single, non-migrating outer giant planet form planets in the Habitable Zone with $\sim 5 \times 10^{-3}$ water by mass (Raymond et al 2004, 2006a). If we assume that previous simulations would have resulted in water contents similar to the Earth's ($\sim 10^{-3}$ by mass) if depletion were accounted for, then the present simulations should still have about 20 times as much water as the Earth. However, it is possible that previous simulations instead formed planets which would have more water than the Earth because the giant planets in those simulations were on circular orbits rather than mildly eccentric orbits similar to the orbits of our own giant planets (Chambers & Cassen 2002; Raymond et al. 2004). Thus, our current planets may in fact contain significantly more water and are likely to be covered in global oceans several km deep and be veritable “ocean planets” (e.g., Léger et al. (2004)).

The water contents of Habitable Zone planets in simulations with and without gas drag differ by about two orders of magnitude. The reasons for this contrast are tied to the presence of nebular gas, via radial mixing of surviving bodies and in-spiraling of icy planetesimals. Thus, the water contents of our final planetary systems may in fact be dependent on our assumptions about the lifetime and depletion of the gas disk and the effective mass of planetesimals. For instance, if gas disk dissipation is the halting mechanism of the giant planet migration (as assumed by, e.g., Trilling et al. (1998)), then perhaps only a Jupiter-mass or so of gas remains at the end of migration. We expect that re-circularization of scattered material and inward migration of small bodies would continue to take place to some extent in such a disk, such that a significant fraction of material would survive to repopulate the terrestrial zone. Thus, the amount of material accreted from the outer system by planets in the interior of the disk would be less. The terrestrial planets in such systems would probably represent an intermediate case between our simulations with and without drag, with moderate masses and water contents. As shown by the final configurations, we can expect that such systems would form habitable planets similar to those formed here.

4. EARTH-LIKE PLANETS IN KNOWN PLANETARY SYSTEMS

It has been shown that an Earth-like planet would be dynamically stable for long timescales in the Habitable

Zones of many of the known systems of giant planets (e.g., Menou & Tabachnik (2003); Jones et al. (2005)). However, these studies only test the stability of existing particles over long timescales; it is assumed that initially-stable objects would form in-situ. This is not the case in moderately unstable environments; stability models predict the existence of an Earth-mass planet at ~ 3 AU in the our system's Asteroid Belt, where such a planet would indeed be dynamically stable. Clearly, when assessing the potential for a viable location for habitable planets it is critical to model the actual formation process.

Our results can be applied to constrain which of the known systems of extra-solar giant planets could have formed a terrestrial planet in the Habitable Zone. By combining limits on formation of terrestrial planets in the presence of various giant planet scenarios, we can make a more rigorous assessment of the possibility for terrestrial planets in known planetary systems and begin to develop criteria for a habitable system. In this section we combine limits on the formation of terrestrial planets in the presence of various giant planet scenarios from this study and a previous study, and assess of the probability of the formation of terrestrial planets in known planetary systems.

Examining the typical spacing between terrestrial and inner giant planets in our simulations, we find that a giant planet must be interior to approximately 0.5 AU for a planet at the lower limit of habitability ($\sim 0.3 M_{\oplus}$; Williams et al. (1997)) to form inside the outer boundary of the Habitable Zone (we have assumed the outer edge of the Habitable Zone to be 1.5 AU, although this value is uncertain and depends on the condensation properties of CO_2 clouds (Kasting et al. 1993; Forget & Pierrehumbert 1997; Mischna et al. 2000)). The spacing of planets that form exterior to the close-in giant varies a great deal from simulation to simulation. In dynamical terms, what is relevant is the ratio of orbital periods of the innermost planet with significant mass ($>0.3 M_{\oplus}$) and the close-in giant planet. This value ranges from 3.3 to 43 in our simulations, with a mean [median] of 12[9]. Although there clearly exists a range of outcomes, we can define a rough limit on the orbit of an inner giant planet that allows a terrestrial planet to form in the Habitable Zone (the most optimistic case, i.e. the closest spacing, puts the giant planet at about 0.7 AU).

We suggest that terrestrial planets of significant mass can form in the Habitable Zone of a Sun-like star if no giant planets exist between 0.5 and 2.5 AU. We derive these values using the reasoning above based on our current results, in combination with the results of Raymond (2006), who used hundreds of low-resolution accretion simulation to constrain which outer giant planets can form Habitable Zone planets (see Fig. 2 from that paper). These values are clearly eccentricity dependent – the characteristic spacing between giant and terrestrial planets increases quickly with giant planet eccentricity (e.g., Raymond (2006)). The highest eccentricity of the close-in giant planets in our simulation is about 0.1, and this value is similar for most simulations. For our inner limit, we therefore assume that a system with a giant planet inside 0.5 AU and with an eccentricity less than 0.1 can form a planet in the Habitable Zone.

We apply these rough limits to the known extrasolar planets. Our sample consists of 207 planets in 178 planetary systems (with 21 multiple planet systems) discovered by Aug 1 2006. We include planets discovered via the radial velocity, micro-lensing, transit and direct imaging techniques (data from Butler et al. (2006) via exoplanets.org, and Schneider (2006) via exoplanet.eu). We exclude planets more massive than 15 Jupiter masses (M_J ; roughly the brown dwarf limit), unless they are part of multiple systems. Because the extrasolar planet host stars have a range in masses, we must calibrate our limits. To do so, we use a mass-luminosity relation that is a fit to data of Hillenbrand & White (2004):

$$y = 4.101x^3 + 8.162x^2 + 7.108x + 0.065, \quad (10)$$

where $y = \log_{10}(L_\star/L_\odot)$ and $x = \log_{10}(M_\star/M_\odot)$ (John Scalo 2006, personal communication). We assume a Habitable Zone of 0.8-1.5 AU around a solar-mass star, and assume that its inner and outer limits scale with the stellar flux, i.e., as $L_\star^{1/2}$. We then assume that the dynamical scaling between the Habitable Zone and our giant planet limits, measured in terms of orbital period ratios, is independent of stellar mass. Table 7 lists our inner and outer giant planet limits for a range of stellar masses.

Figure 12 shows the known extrasolar planets that meet our criteria and are good candidates for having a terrestrial planet in the Habitable Zone. Potentially habitable systems are also listed in Table 8, sorted by host star mass. Of the 178 systems in our sample, 65 (37%) may have formed a terrestrial planet of $0.3 M_\oplus$ or more in the Habitable Zone and so are considered to be potentially habitable systems. Seventeen systems satisfy our outer giant planet limit; these are Solar System-like in that they have a giant planet exterior to the Habitable Zone. In contrast, fifty systems are decidedly different than the Solar system, with the potential for an Earth-like planet coexisting with a close-in giant planet. One system, 55 Cancri, falls into both categories, with three close-in giants and a distant outer giant. Nine of the multiple planet systems contained a planet that satisfied our limits but another planet that did not – 55 Cnc was the only multiple system for which all planets met our limits. If we consider the ensemble of planets as a whole, then 75 out of 207 planets (36 %) met our criteria. In the case of planets at very large orbital distances, such as the ones detected by direct imaging (e.g., Chauvin et al. (2005)), the giant planet is so far away that it will be completely dynamically detached from the terrestrial region.

Our estimate that about one third of the known giant planet systems can harbor potentially habitable planets diverges from previous estimates. Jones et al. (2005) used the stability of Earth-mass test particles to suggest that about half of the known systems could contain a planet in the Habitable Zone. As noted above, the stability of a given region does not always imply that a planet exists in the region – the Asteroid Belt is a convenient example of a stable region that contains no Earth-mass planet. We suspect that the difference between our estimate and that of Jones et al. (2005) are a number of systems in which stable regions exist but planets are unlikely to form. This is not unexpected; for example, Barnes & Raymond (2004) found stable regions for test particles in four known extrasolar planetary systems, but

Raymond et al. (2006a) showed that sizable terrestrial planets could only accrete in two of the systems.

Conversely, in previous work studying the formation of planets in systems with one giant planet exterior to the terrestrial planets (Raymond 2006) we concluded that only 5% of the known giant planet systems could form planets of at least $0.3 M_\oplus$ in the Habitable Zone. Our current estimate has increased to roughly one third, because of two factors: 1) our sample is larger than in Raymond (2006), and 2) we have determined that many inner giant planet systems could form Earth-like planets in the Habitable Zone. Given that observational biases make it much easier to find close-in giant planets, it is not surprising that our estimate for the number of habitable systems has increased.

In this analysis, we have only considered a few key parameters – stellar mass, planet semi-major axis and eccentricity. Table 8 also lists the other parameters which we consider most important in terms of habitable planet formation: planetary mass and stellar metallicity. Perturbations from lower (higher)-mass planets are correspondingly weaker (stronger), so for less (more) massive giant planets our inner limit would move out (in), and our outer limit would move in (out). With the increasing number of lower-mass extrasolar planets being discovered (e.g., Butler et al. (2004); Lovis et al. (2006)), we suspect that our limits are relatively conservative for the population of extrasolar planets as a whole. The median mass of our sample is $0.76 M_{Jup}$, so our limits are appropriate on a statistical level. The stellar metallicity is thought to be related to the gas- to dust ratio of the disk and therefore the total mass in terrestrial building blocks. In addition, if the disk mass scales with stellar mass (as is generally thought), there may be a deficit of rocky material and perhaps fewer Earth-like planets around low-mass stars (Raymond et al. 2006d).

The next generations of space missions plan to discover and characterize Earth-like planets around other stars. These missions include NASA's *Kepler*, *SIM* and *Terrestrial Planet Finder*, and CNES's *COROT* and ESA's *Darwin*. Our results suggest that terrestrial planets can coexist with both close-in giant planets and giant planets in outer orbits, expanding the range of planetary systems that should be searched with these upcoming missions. However, transit searches are very sensitive to orbital inclination. In many cases our simulated Habitable Zone planets have mutual inclinations of 5-10° with respect to the orbit of the close-in giant planet, making detection of transits for both planets impossible. Final inclinations are smaller for systems with an exterior giant planet, making systems with both an exterior and interior giant planet more amenable to detection, but overall the probability of seeing the transit of a close-in giant planet and a HZ planet in the same system is small. However, transit timing measurements may be able to infer the presence of HZ planets in these systems (Holman & Murray 2005; Agol et al. 2005).

5. CONCLUSION

5.1. Summary

Our simulations demonstrate that terrestrial accretion can occur during and after giant planet migration on several fronts:

1. Interior to the migrating giant planet, planetesimals and embryos are shepherded inward by the combined effects of moving mean motion resonances and dissipation via gas drag (Tanaka & Ida (1999); also shown by Fogg & Nelson (2005) and Zhou et al. (2005)). Rapid accretion occurs over the duration of migration (Stage 1), and 40%–50% of material inside 5 AU typically ends up in the form of 1 - 3 “hot Earths” when a gaseous disk is present. These planets have masses up to 5 M_{\oplus} and accrete on the migration timescale of 10^5 years. Hot Earths tend to lie inside strong resonances such as the 2:1 and 3:2. Planetesimals, which feel stronger drag, can be shepherded by higher-order resonances.
2. Exterior to the giant planet, scattered embryos and planetesimals have their orbits re-circularized by damping from gas drag (felt more strongly by planetesimals) and dynamical friction (felt by embryos due to the planetesimals) during Stage 2. The embryos in this region begin with compositions similar to the initial mean composition, but an influx of material into the terrestrial zone (between the close-in giant and 2.5 AU) from orbital decay of planetesimals due to gas drag can significantly enhance the masses and fraction of water-rich material in these bodies. From these protoplanets a system of terrestrial planets forms on a $\sim 10^8$ year timescale after the gas disk has dissipated (Stage 3).
3. In the outer disk, damping via both gas drag and dynamical friction is much weaker. Thus, a scattered disk of planetesimals and embryos remain on high eccentricity and inclination orbits, similar to the scattered disk of comets in the solar system (Luu et al. 1997; Duncan & Levison 1997). Timescales for accretion are very long. The presence of a second giant planet serves to remove dynamically hot bodies, diminishing the orbital excitation of bodies and reducing the clearing time in the outer system.

Planets formed in the Habitable Zone in a significant fraction of our simulations. These planets have masses and orbits similar to those seen in previous simulations including only outer giant planets (Chambers 2001; Raymond et al. 2004, 2006c). However, Habitable Zone planets in systems with close-in giant planets tend to accrete a much larger amount of water than those in systems with only outer giant planets (Raymond et al. 2006b). The reason for these high water contents is twofold: 1) strong radial mixing is induced by the giant planet’s migration, and 2) in-spiraling icy planetesimals are easily accreted by planets in the terrestrial zone. Although we have not taken water depletion into account, these planets contain about **twenty** times as much water as those formed in similar outer giant planet simulations (Raymond et al. 2004, 2006c). These planets are likely to be “water worlds”, covered in kilometers-deep global oceans (Léger et al. 2004).

The variations in the evolutionary process for each of the three models examined here demonstrate the impor-

tance of both the configuration of giant planets in the system as well as the presence and duration of the gaseous disk in dictating the final parameters of the terrestrial planets formed. Simulations run without including the gaseous disk (JSN) showed very little planetesimal accretion during migration and almost no collisions after migration due to the strong dynamical excitation of the disk (see Figure 7). Though embryo eccentricities and inclinations decreased due to dynamical friction, the mean embryo composition remained similar to the initial value and final terrestrial planet masses were in the lower end of the mass range seen in the Solar System (see Figure 11). In contrast, embryos in simulations including the presence of a dissipating gaseous disk (JD and JSD) accreted planetesimals and other embryos from both the inner system (during Stage 1) and the outer system (during Stage 2). This resulted in both higher planet masses and water mass fractions, though this effect was slightly mitigated in the JSD simulations due to more rapid clearing in the outer system. Eccentricities and inclinations are also affected by the presence of an outer giant planet; in the JD simulations dynamical excitation continues unabated during Stage 3, while in the JSD simulations excited bodies are scattered by the Saturn-mass planet and the remaining bodies therefore remain dynamically relaxed.

5.2. Implications for Our Own System

If planetary systems which suffer the migration of a giant planet to small distances can eventually form terrestrial planets similar to those in our own system, and the migration of young giant planets is a common result of interactions with the gaseous disk, then it is appropriate to consider the possibility that our own planetary system could have formed earlier generations of giant planets prior to those in the outer Solar System. The systems simulated here undergo extensive radial mixing of large bodies throughout the inner and outer system through scattering, which could leave a elemental signature on the final population of both planetary and sub-planetary bodies. However, radial mixing of dust and smaller bodies is also thought to occur through a variety of other processes in the planet formation region besides planetary scattering (see Wooden et al. (2005) for a detailed discussion), and it is clear from the final abundances of planets in our simulations and others that any signature of the scattering of massive bodies early in the formation history will be quickly erased through accretion in the inner system due to continued mixing. This is less true in the outer system, where long dynamical timescales and low solid and gas densities make accretion and radial transport less likely. Therefore one of the primary constraints on giant planet formation and migration theories is the scattered population of Kuiper Belt objects (KBO’s) and Oort Cloud comets – both their orbital and compositional characteristics.

Though conclusive detection of anomalous cometary and asteroidal abundances is naturally difficult and ambiguous, the detection of comet-like bodies with orbital characteristics suggesting an origin in the Oort Cloud but with physical appearances similar to asteroids could be considered a strong indicator of the scattering of massive inner-disk bodies by a migrating giant planet. In fact, such bodies (known as Damocloids) have recently

been discovered (Asher et al. 1994; Jewitt 2005), but it is unclear whether any of these bodies are truly asteroidal in composition, and even if they are it has been shown that the stochastic nature of late-stage scattering by Jupiter could also produce small numbers of Oort Cloud comets of asteroidal nature (Weissman & Levison 1997). A more conclusive sign of giant planet migration would be a classical KBO with a composition primarily composed of refractory materials; this would imply the re-circularization of a scattered inner-disk object, which would most likely only be possible in the presence of damping by significant amounts of gas or dust for long timescales. In-depth analysis of the meteoritic and cometary record and other signatures of long-term planetary dynamics for evidence of early giant planet migration is clearly beyond the scope of this paper, and would most likely be inconclusive considering the many factors involved. We must wait for the detection and accurate analysis of many more KBO's and Oort Cloud comets before we can place meaningful constraints on the possibility of Type II giant planet migration in our own system.

5.3. Future Work

In this study we have endeavored to utilize the most concrete data and plausible scenarios to develop our initial conditions for each model, while limiting the number of free parameters and ill-constrained variables. However, there is naturally a range of parameter space in the formation of terrestrial planets in systems with a migrating giant planet that we could not explore.

We have only considered systems with one migrating giant planet. The observed distribution of giant planet orbital parameters can be roughly reproduced by the combination of migration and gravitational scattering (e.g., Adams & Laughlin (2003)). Thus, in certain cases there may be multiple giant planets migrating together. Simulations by Bryden et al. (2000) and Kley (2000) suggest that if the planets attain their full mass while on closely-spaced orbits, the intervening gas between them would cause convergent migration, leading to resonance capture or scattering. However, if one planet forms sufficiently early to migrate inwards, a second planet could form beyond the evacuation zone and migrate as well. In this case gravitational scattering would be greatly enhanced because inner disk material would interact with both giant planets and would probably be scattered to larger orbital distances (as occurs for some bodies in model JSD). However, in most cases the dynamic instabilities of the two massive planets would likely outweigh the evolution of the smaller bodies, leading to chaotic scattering and removal of small bodies similar as out-

lined in Veras & Armitage (2005). If a combined migration leaves one planet in a small orbit within 0.5 AU and a second planet beyond 2 AU, one would expect a hybrid scenario between this work and Raymond (2006) with terrestrial planets forming in the stable region between the two giant planets, but more work is needed to confirm this.

Additional uncertainty surrounds the role of the gaseous disk. In this work we bracket the potential range of disk masses with the JSD and JSN models. As stated, the differences in the damping of scattering energies and the orbital decay of planetesimal orbits greatly impacts the final characteristics of the terrestrial planets that are formed. To fully investigate the full range of gas disk properties and planetesimal size ranges would require an unreasonably large number of simulation runs. Our simulations were limited by computational resources. We chose fixed values for several parameters such as the migration rate and disk properties, and chose to integrate these simulations for a long time rather than explore the effects of different parameters. (Note that Fogg & Nelson (2005) explored the effects of the disk's mass distribution.) In addition, we did not include the effects of collisional fragmentation, which are certainly important for both planetesimal- (e.g., Benz & Asphaug (1999) and embryo-scale collisions (Asphaug et al. 2006)). More effects relating to the gas disk also remain to be modeled, including tidal gas drag (e.g., Kominami & Ida (2002)), which acts preferentially on larger bodies. Clearly, more work remains to include all of the relevant physics. Despite these limitations, our simulations are among the first to realistically address this problem and examine the final results of terrestrial planet formation under these conditions (also see earlier work: Mandell & Sigurdsson (2003); Fogg & Nelson (2005); Zhou et al. (2005); Paper 1; Fogg & Nelson (2006)). Hopefully this work will encourage future studies to expand and improve the models explored here, both in our understanding of the relevant physical conditions and our ability to realistically model the myriad and complex forces at work in the formation of terrestrial planetary systems.

6. ACKNOWLEDGMENTS

We thank NASA Astrobiology Institute for funding, through the Penn State (A.M. and S.S.), NASA Goddard (A.M.), Virtual Planetary Laboratory (S.R.) and University of Colorado (S.R.) lead teams. Thanks also to John Scalo for providing our mass-luminosity relation. S.N.R. was partially supported by an appointment to the NASA Postdoctoral Program at the University of Colorado Astrobiology Center, administered by Oak Ridge Associated Universities through a contract with NASA.

REFERENCES

- Abe, Y., Ohtani, E., Okuchi, T., Righter, K., & Drake, M. 2000, Origin of the earth and moon, edited by R.M. Canup and K. Righter and 69 collaborating authors. Tucson: University of Arizona Press., p.413-433, 413
- Adachi, I., Hayashi, C., & Nakazawa, K. 1976, Progress of Theoretical Physics, 56, 1756
- Adams, F. C., & Laughlin, G. 2003, Icarus, 163, 290
- Agol, E., Steffen, J., Sari, R., & Clarkson, W. 2005, MNRAS, 359, 567
- Alibert, Y., Mordasini, C., Benz, W., & Winisdoerffer, C. 2005, A&A, 434, 343
- Armitage, P. J. 2003, ApJ, 582, L47
- Asher, D. J., Bailey, M. E., Hahn, G., & Steel, D. J. 1994, MNRAS, 267, 26
- Asphaug, E., Agnor, C. B., & Williams, Q. 2006, Nature, 439, 155
- Barnes, R., & Raymond, S. N. 2004, ApJ, 617, 569
- Beaulieu, J.-P., et al. 2006, Nature, 439, 437
- Beckwith, S. V. W., Henning, T., & Nakagawa, Y. 2000, Protostars and Planets IV, 533
- Bennett, D. P., Anderson, J., Bond, I. A., Udalski, A., & Gould, A. 2006, ApJ, 647, L171
- Benz, W., & Asphaug, E. 1999, Icarus, 142, 5
- Bodenheimer, P., Hubickyj, O., & Lissauer, J. J. 2000, Icarus, 143, 2

- Bond, I. A., et al. 2004, *ApJ*, 606, L155
- Bonfils, X., et al. 2005, *A&A*, 443, L15
- Boss, A. P. 1997, *Science*, 276, 1836
- Boss, A. P. 1998, *ApJ*, 503, 923
- Boss, A. P. 2000, *ApJ*, 536, L101
- Boss, A. P. 2001, *ApJ*, 563, 367
- Boss, A. P. 2005, *ApJ*, 629, 535
- Briceño, C., et al. 2001, *Science*, 291, 93
- Bryden, G., Różyczka, M., Lin, D. N. C., & Bodenheimer, P. 2000, *ApJ*, 540, 1091
- Bryden, G., et al. 2006, *ApJ*, 636, 1098
- Butler, R. P., Vogt, S. S., Marcy, G. W., Fischer, D. A., Wright, J. T., Henry, G. W., Laughlin, G., & Lissauer, J. J. 2004, *ApJ*, 617, 580
- Butler, R. P., et al. 2006, *ApJ*, 646, 505
- Calvet, N., Muzerolle, J., Briceño, C., Hernández, J., Hartmann, L., Saucedo, J. L., & Gordon, K. D. 2004, *AJ*, 128, 1294
- Canup, R. M., & Pierazzo, E. 2006, 37th Annual Lunar and Planetary Science Conference, 37, 2146
- Carroll, B. W., & Ostlie, D. A. 1996, *An Introduction to Modern Astrophysics*, by B.W. Carroll and D.A. Ostlie. Benjamin Cummings, 1996.
- Chiang, E. I., Fischer, D., & Thommes, E. 2002, *ApJ*, 564, L105
- Chambers, J. E., & Migliorini, F. 1997, *BAAS*, 29, 1024
- Chambers, J. E. 1999, *MNRAS*, 304, 793
- Chambers, J. E. 2001, *Icarus*, 152, 205
- Chambers, J. E., & Cassen, P. 2002, *Meteoritics and Planetary Science*, 37, 1523
- Chauvin, G., et al. 2005, *A&A*, 438, L29
- Ciesla, F. J., & Cuzzi, J. N. 2006, *Icarus*, 181, 178
- D'Angelo, G., Kley, W., & Henning, T. 2003, *ApJ*, 586, 540
- Duncan, M. J., & Levison, H. F. 1997, *Science*, 276, 1670
- Durisen, R. H., Cai, K., Mejía, A. C., & Pickett, M. K. 2005, *Icarus*, 173, 417
- Edgar, R., & Artymowicz, P. 2004, *MNRAS*, 354, 769
- Eisner, J. A., Hillenbrand, L. A., White, R. J., Akeson, R. L., & Sargent, A. I. 2005, *ApJ*, 623, 952
- Farinella, P. 1980, *Moon and Planets*, 22, 25
- Fernandez, J. A., & Ip, W.-H. 1984, *Icarus*, 58, 109
- Fischer, D. A., & Valenti, J. 2005, *ApJ*, 622, 1102
- Fogg, M. J., & Nelson, R. P. 2005, *A&A*, 441, 791
- Fogg, M. J., & Nelson, R. P. 2006, *A&A*, in press
- Forget, F., & Pierrehumbert, R. T. 1997, *Science*, 278, 1273
- Gammie, C. F. 1996, *ApJ*, 457, 355
- Genda, H., & Abe, Y. 2005, *Nature*, 433, 842
- Goldreich, P., & Ward, W. R. 1973, *ApJ*, 183, 1051
- Golimowski, D. A., et al. 2006, *AJ*, 131, 3109
- Gonzalez, G., Brownlee, D., & Ward, P. 2001, *Icarus*, 152, 185
- Gould, A., et al. 2006, *ApJ*, 644, L37
- Greenberg, R., Hartmann, W. K., Chapman, C. R., & Wacker, J. F. 1978, *Icarus*, 35, 1
- Grossman, L. 1972, *Geochim. Cosmochim. Acta*, 36, 597
- Guillot, T. 1999, *Planet. Space Sci.*, 47, 1183
- Hahn, J. M., & Malhotra, R. 1999, *AJ*, 117, 3041
- Haisch, K. E., Jr., Lada, E. A., & Lada, C. J. 2001, *ApJ*, 553, L153
- Hayashi, C. 1981, *Progress of Theoretical Physics Supplement*, 70, 35
- Hillenbrand, L. A., & White, R. J. 2004, *ApJ*, 604, 741
- Holman, M. J., & Murray, N. W. 2005, *Science*, 307, 1288
- Hubickyj, O., Bodenheimer, P., & Lissauer, J. J. 2005, *Icarus*, 179, 415
- Jewitt, D. 2005, *AJ*, 129, 530
- Jones, B. W., Underwood, D. R., & Sleep, P. N. 2005, *ApJ*, 622, 1091
- Kasting, J. F., Whitmire, D. P., & Reynolds, R. T. 1993, *Icarus*, 101, 108
- Kenyon, S. J., & Bromley, B. C. 2006, *AJ*, 131, 1837
- Kleine, T., Münker, C., Mezger, K., & Palme, H. 2002, *Nature*, 418, 952
- Kley, W. 2000, *MNRAS*, 313, L47
- Kokubo, E., & Ida, S. 1995, *Icarus*, 114, 247
- Kokubo, E., & Ida, S. 1998, *Icarus*, 131, 171
- Kokubo, E., & Ida, S. 2000, *Icarus*, 143, 15
- Kominami, J., & Ida, S. 2002, *Icarus*, 157, 43
- Laughlin, G., Steinacker, A., & Adams, F. C. 2004, *ApJ*, 608, 489
- Laws, C., Gonzalez, G., Walker, K. M., Tyagi, S., Dodsworth, J., Snider, K., & Suntzeff, N. B. 2003, *AJ*, 125, 2664
- Léger, A., et al. 2004, *Icarus*, 169, 499
- Levison, H. F., & Duncan, M. J. 2000, *AJ*, 120, 2117
- Lin, D. N. C., Bodenheimer, P., & Richardson, D. C. 1996, *Nature*, 380, 606
- Lineweaver, C. H. 2001, *Icarus*, 151, 307
- Lineweaver, C. H., Fenner, Y., & Gibson, B. K. 2004, *Science*, 303, 59
- Lissauer, J. J. 1987, *Icarus*, 69, 249
- Lissauer, J. J. 1993, *ARA&A*, 31, 129
- Lodders, K., & Fegley, B. 1998, *The planetary scientist's companion / Katharina Lodders, Bruce Fegley*. New York : Oxford University Press, 1998.
- Lovis, C., et al. 2006, *Nature*, 441, 305
- Luu, J., Marsden, B. G., Jewitt, D., Trujillo, C. A., Hergenrother, C. W., Chen, J., & Offutt, W. B. 1997, *Nature*, 387, 573
- Mandell, A. M., & Sigurdsson, S. 2003, *ApJ*, 599, L111
- Matsui, T., & Abe, Y. 1986, *Nature*, 322, 526
- Mayer, L., Quinn, T., Wadsley, J., & Stadel, J. 2002, *Science*, 298, 1756
- Mayer, L., Quinn, T., Wadsley, J., & Stadel, J. 2004, *ApJ*, 609, 1045
- Mayor, M., Udry, S., Naef, D., Pepe, F., Queloz, D., Santos, N. C., & Burnet, M. 2004, *A&A*, 415, 391
- McNeil, D., Duncan, M., & Levison, H. F. 2005, *AJ*, 130, 2884
- Menou, K., & Tabachnik, S. 2003, *ApJ*, 583, 473
- Mischna, M. A., Kasting, J. F., Pavlov, A., & Freedman, R. 2000, *Icarus*, 145, 546
- Morbidelli, A., Chambers, J., Lunine, J. I., Petit, J. M., Robert, F., Valsecchi, G. B., & Cyr, K. E. 2000, *Meteoritics and Planetary Science*, 35, 1309
- Moutou, C., et al. 2005, *A&A*, 439, 367
- Murray, N., Hansen, B., Holman, M., & Tremaine, S. 1998, *Science*, 279, 69
- Muzerolle, J., Hillenbrand, L., Calvet, N., Briceño, C., & Hartmann, L. 2003, *ApJ*, 592, 266
- Nelson, R. P., & Papaloizou, J. C. B. 2004, *MNRAS*, 350, 849
- Nordström, B., et al. 2004, *A&A*, 418, 989
- Owen, T., & Bar-Nun, A. 1995, *Icarus*, 116, 215
- Papaloizou, J., & Lin, D. N. C. 1984, *ApJ*, 285, 818
- Papaloizou, J. C. B., & Terquem, C. 2006, *Reports of Progress in Physics*, 69, 119
- Pepe, F., et al. 2004, *A&A*, 423, 385
- Pollack, J. B., Hubickyj, O., Bodenheimer, P., Lissauer, J. J., Podolak, M., & Greenzweig, Y. 1996, *Icarus*, 124, 62
- Rasio, F. A., & Ford, E. B. 1996, *Science*, 274, 954
- Raymond, S. N., Quinn, T., & Lunine, J. I. 2004, *Icarus*, 168, 1
- Raymond, S. N., Quinn, T., & Lunine, J. I. 2005, *Icarus*, 177, 256
- Raymond, S. N. 2006, *ApJ*, 643, L131
- Raymond, S. N., Barnes, R., & Kaib, N. A. 2006, *ApJ*, 644, 1223
- Raymond, S. N., Mandell, A. M., & Sigurdsson, S. 2006, *Science*, 313, 1413.
- Raymond, S. N., Quinn, T., & Lunine, J. I. 2006, *Icarus*, 183, 265
- Raymond, S. N., Scalzo, J., & Meadows, V. S. 2006, *ApJL*, submitted.
- Reid, N., & Hawley, S. L. 2000, *New light on dark stars : red dwarfs, low mass stars, brown dwarfs / Neill Reid and Suzanne L. Hawley*. New York : Springer, 2000.
- Rice, W. K. M., & Armitage, P. J. 2003, *ApJ*, 598, L55
- Rice, W. K. M., Lodato, G., Pringle, J. E., Armitage, P. J., & Bonnell, I. A. 2004, *MNRAS*, 355, 543
- Saunon, D., & Guillot, T. 2004, *ApJ*, 609, 1170
- Schneider, J. *The Extrasolar Planets Encyclopedia* (available at <http://www.obspm.fr/encycl/encycl.html>)
- Silverstone, M. D., et al. 2006, *ApJ*, 639, 1138
- Stepinski, T. F., & Valageas, P. 1997, *A&A*, 319, 1007
- Stevenson, D. J., & Lunine, J. I. 1988, *Icarus*, 75, 146
- Tabachnik, S., & Tremaine, S. 2002, *MNRAS*, 335, 151
- Tanaka, H., & Ida, S. 1999, *Icarus*, 139, 350
- Tanaka, H., Takeuchi, T., & Ward, W. R. 2002, *ApJ*, 565, 1257
- Thommes, E. W., Duncan, M. J., & Levison, H. F. 2003, *Icarus*, 161, 431
- Thommes, E. W. 2005, *ApJ*, 626, 1033
- Trilling, D. E., Benz, W., Guillot, T., Lunine, J. I., Hubbard, W. B., & Burrows, A. 1998, *ApJ*, 500, 428
- Udalski, A., et al. 2005, *ApJ*, 628, L109
- Veras, D., & Armitage, P. J. 2005, *ApJ*, 620, L111
- Ward, W. R. 1993, *Icarus*, 106, 274
- Ward, W. R. 1997, *Icarus*, 126, 261
- Wetherill, G. W., & Stewart, G. R. 1989, *Icarus*, 77, 330
- Wetherill, G. W. 1996, *Icarus*, 119, 219
- Weidenschilling, S. J. 1977, *MNRAS*, 180, 57
- Weidenschilling, S. J., & Marzari, F. 1996, *Nature*, 384, 619
- Weidenschilling, S. J., Spaute, D., Davis, D. R., Marzari, F., & Ohtsuki, K. 1997, *Icarus*, 128, 429
- Weissman, P. R., & Levison, H. F. 1997, *ApJ*, 488, L133
- Williams, D. M., Kasting, J. F., & Wade, R. A. 1997, *Nature*, 385, 234
- Wooden, D. H., Harker, D. E., & Brearley, A. J. 2005, *ASP Conf. Ser.* 341: Chondrites and the Protoplanetary Disk, 341, 774
- Youdin, A. N., & Shu, F. H. 2002, *ApJ*, 580, 494
- Zhou, J.-L., Aarseth, S. J., Lin, D. N. C., & Nagasawa, M. 2005, *ApJ*, 631, L85
- Zucker, S., Mazeh, T., Santos, N. C., Udry, S., & Mayor, M. 2004, *A&A*, 426, 695

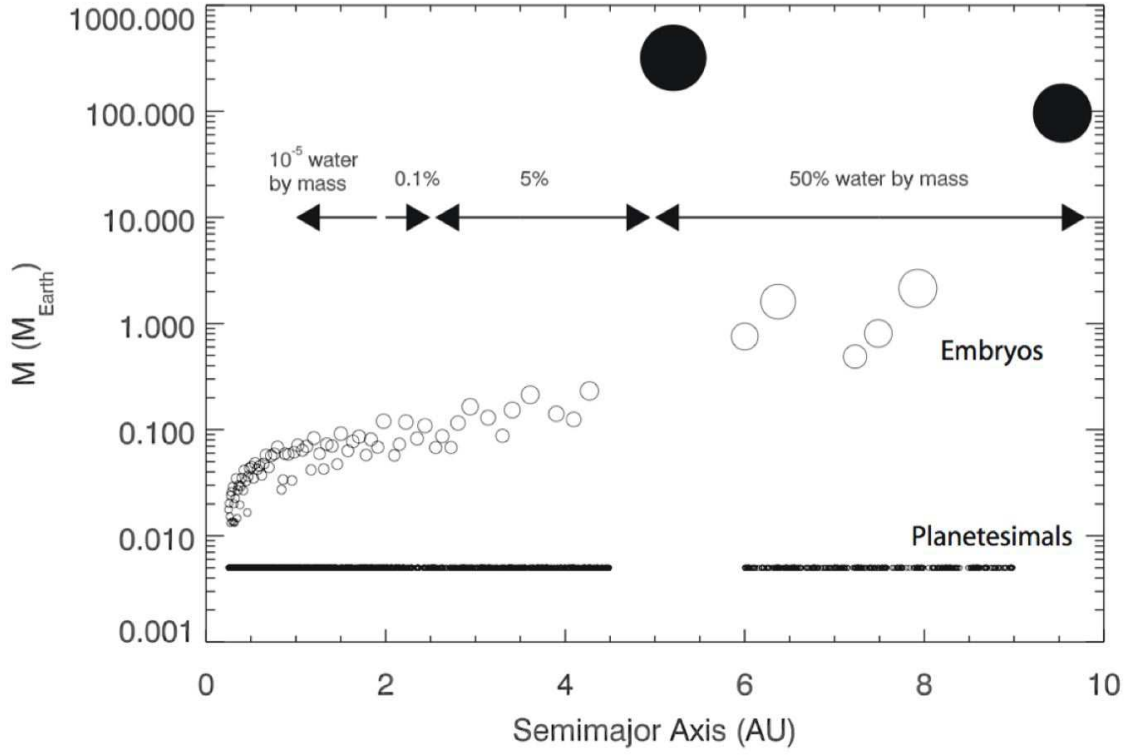


FIG. 1.— Initial values for the mass and water mass fraction of protoplanetary disk used for each simulation. The solid disk is modeled after the Hayashi (1981) MMSN, augmented by a factor of 2.2. Embryos are spaced randomly by $\Delta=5-10$ mutual Hill radii, and embryo masses increase with radial distance r as $M_{emb} \propto \Delta^{3/2} r^{3/4}$. Water and iron contents are based on measurements from Solar System bodies (Abe et al. 2000; Lodders & Fegley 1998).

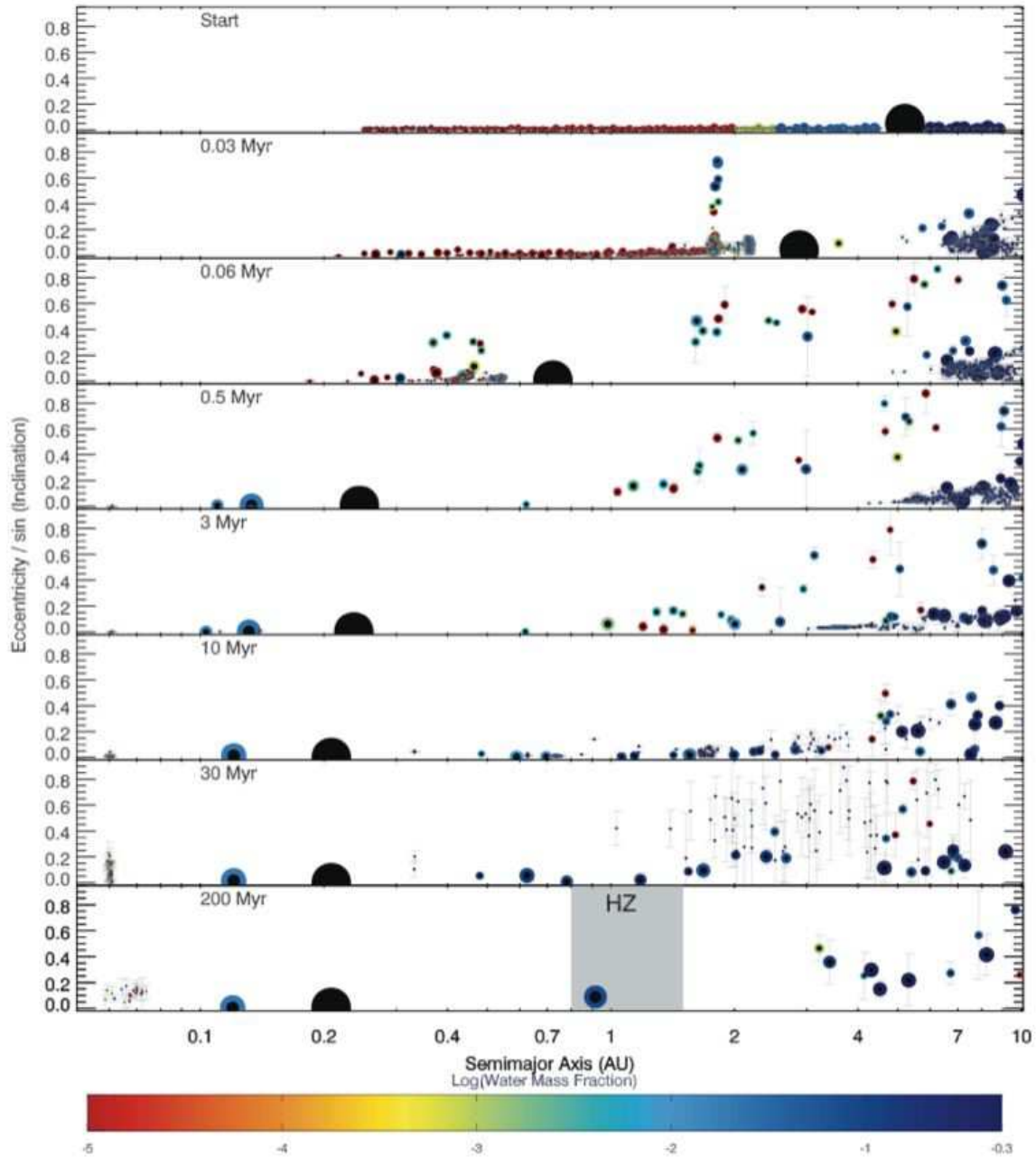


FIG. 2.— Evolution of a sample simulation run using the JD model (a single migrating Jupiter-mass planet with gas drag included). Radial distance is plotted on the x-axis, with eccentricity on the y-axis. Relative inclination is indicated through error-bars on each point, and water content is indicated by the color (a reference bar is located below the plot). The size of each point is proportional to $M^{1/3}$, with the size of the inner black region representing the iron mass fraction. The system forms a 'hot Earth' and a massive terrestrial planet in the Habitable Zone. Water contents are high through radial mixing and migration of planetesimals. Reprinted from Raymond et al. (2006b) (Paper I).

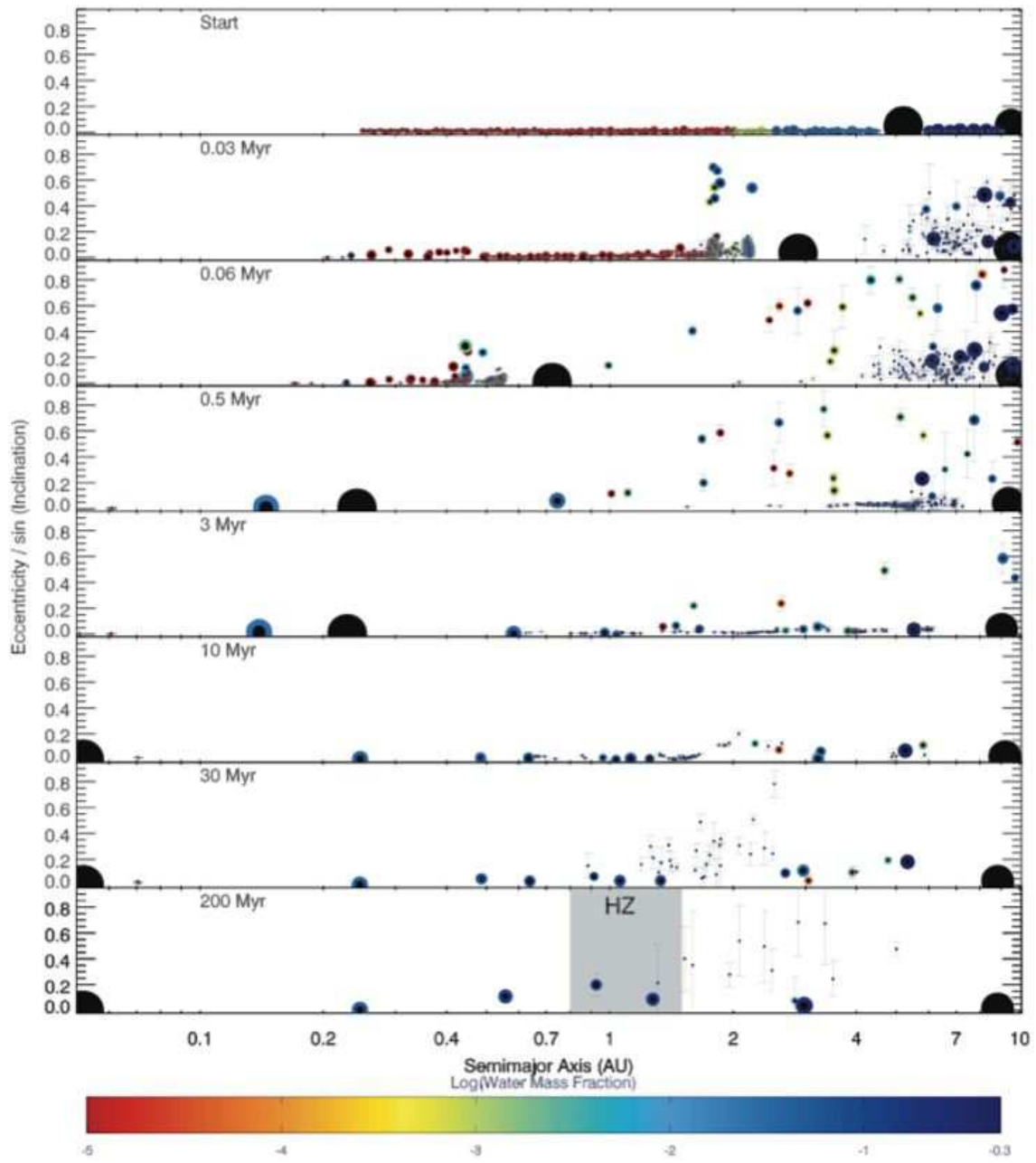


FIG. 3.— Evolution of a sample simulation run using the JSD model (a migrating Jupiter-mass planet with a second Saturn-mass outer planet and gas drag included). The evolution on the inner system is similar to the JD model, but the outer system is cleared rapidly and less water-rich material flows into the inner system.

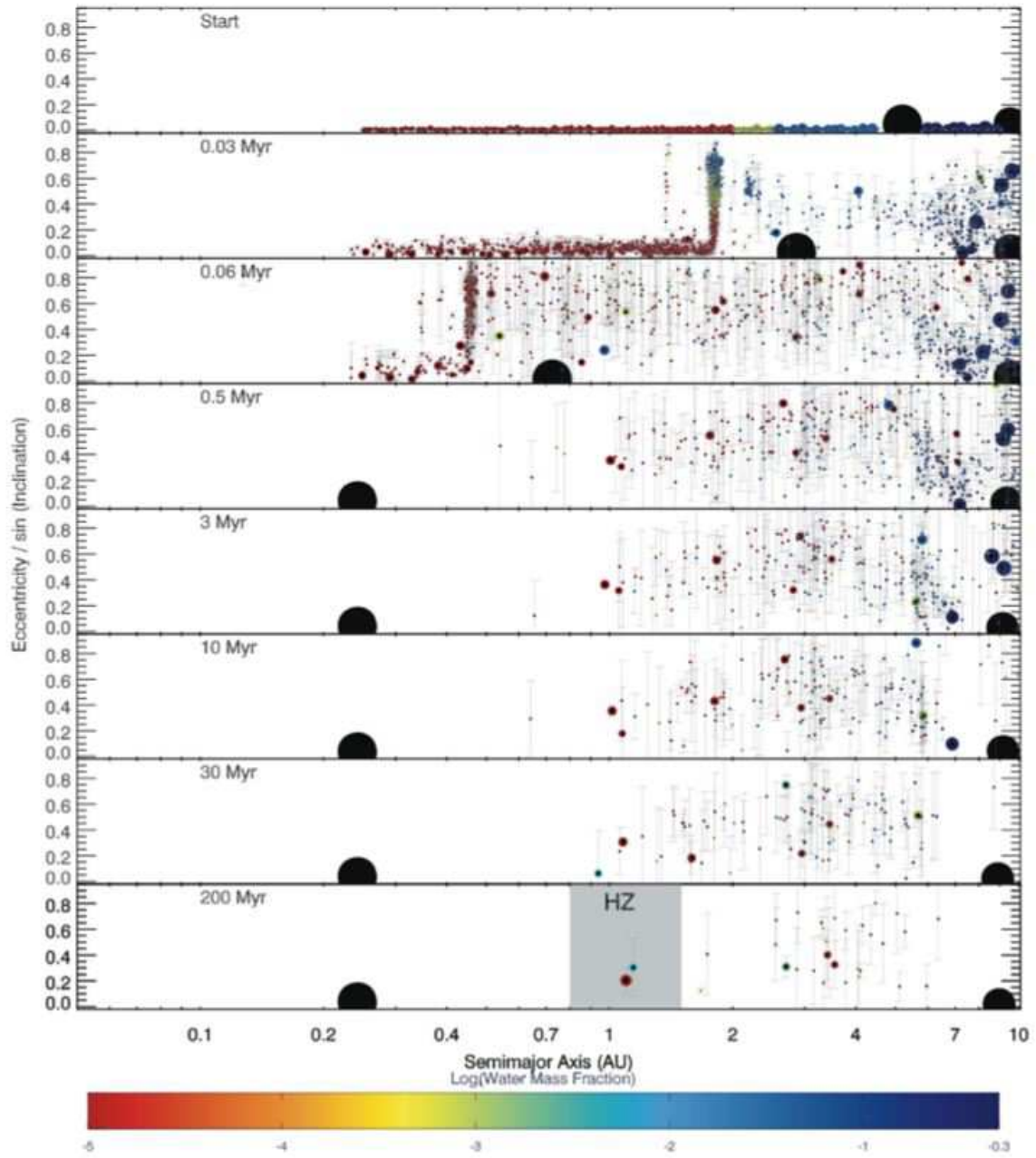


FIG. 4.— Evolution of a sample simulation run using the JSN model (a migrating Jupiter-mass planet with a second Saturn-mass outer planet and no gas drag). The protoplanetary disk is highly excited, with most of the mass being lost to ejection. Over long time scales dynamical friction cools the disk, and low-mass planets with lower water contents form.

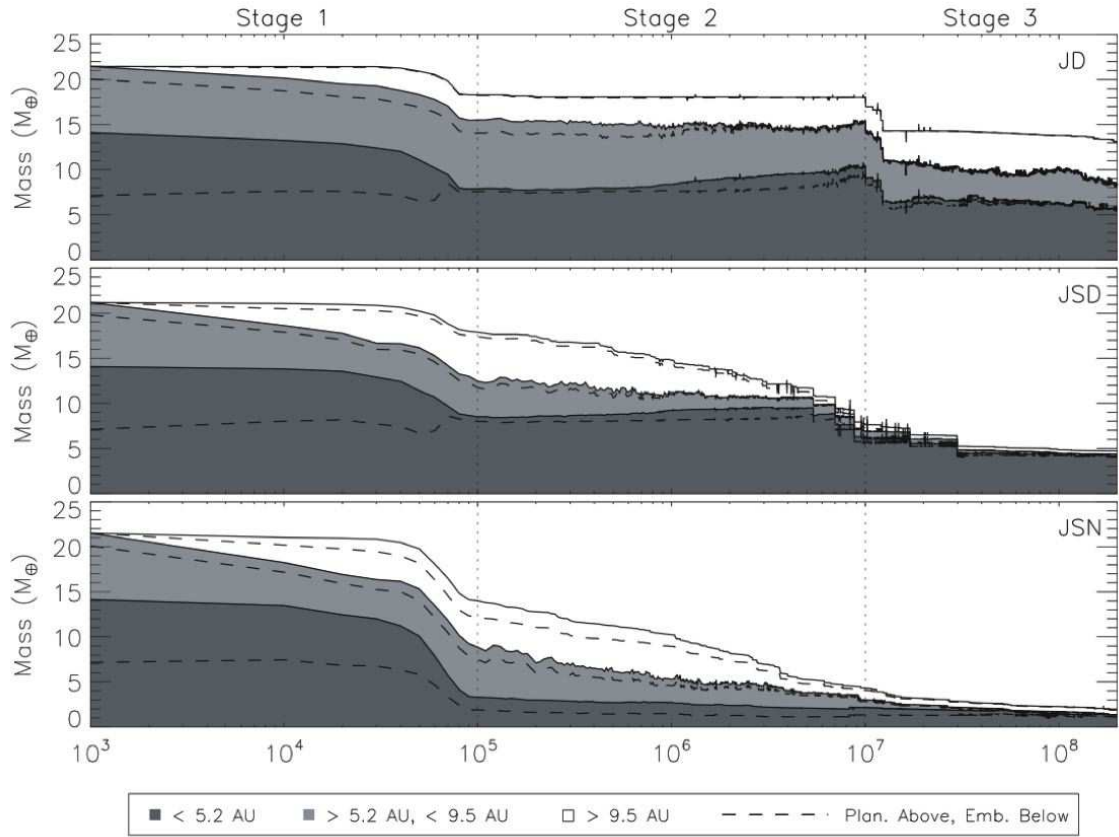


FIG. 5.— The average total mass of the three models (in M_{\oplus}) versus time. The total mass is divided into three zones: the inner disk ($a < 5.2 \text{ AU}$), the intermediate disk ($5.2 \text{ AU} \leq a < 9.5 \text{ AU}$), and the outer disk ($a > 9.5 \text{ AU}$). Additionally, a dashed line is placed at the embryo / planetesimal mass boundary - below the line is the mass from embryos, above it is the mass from planetesimals. Differences can be seen between the three models, specifically in the loss of mass without the presence of gas and the rapid evolution of the outer disk with the presence of a second giant planet.

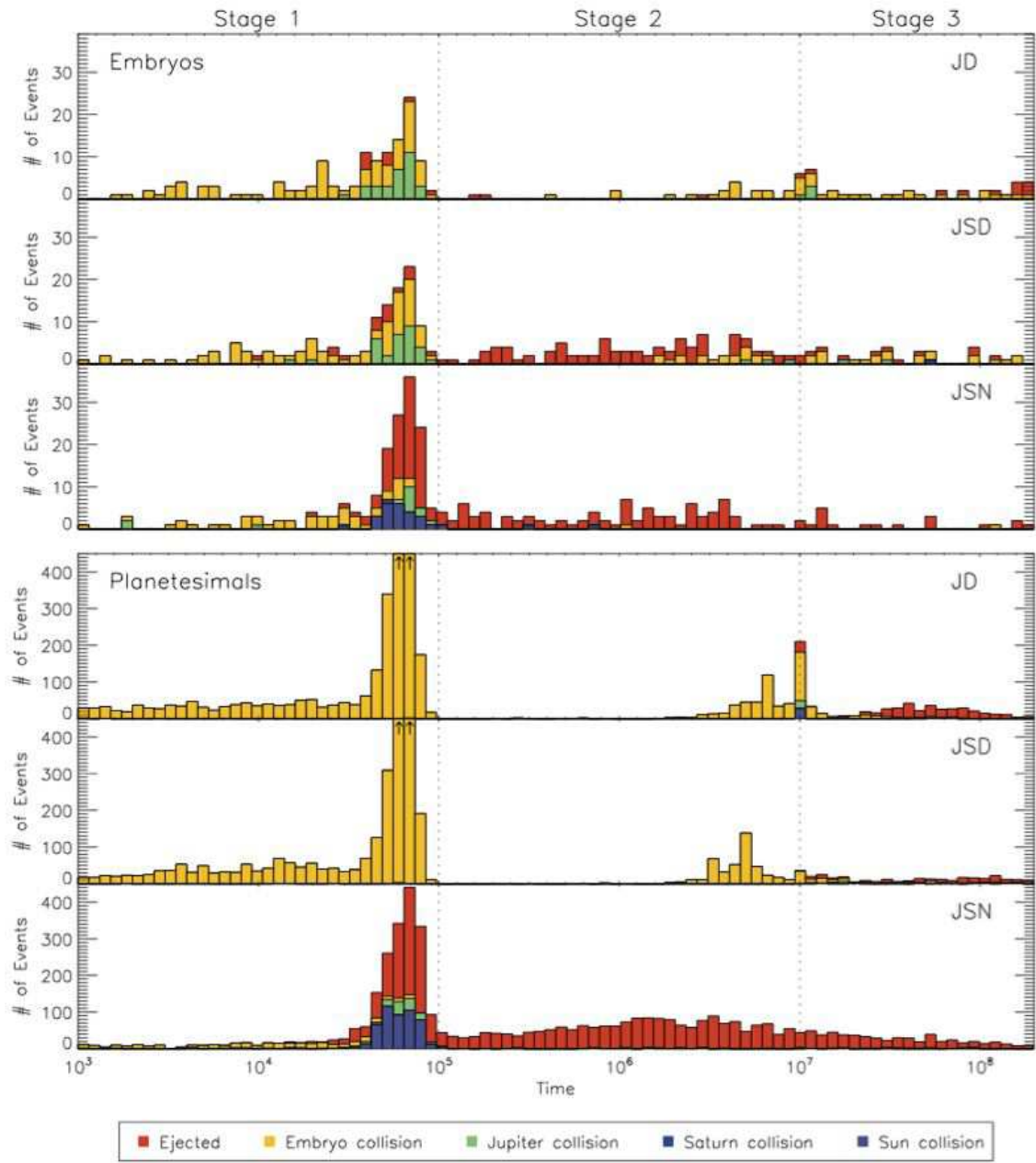


FIG. 6.— Illustration of the loss processes for embryos and planetesimals over time for the three models. Accretion happens primarily during migration, with additional accretion occurring as the gas disappears at 10 Myr. Simulations with gas drag show almost complete accretion onto embryos and Jupiter at early times, then JSD simulations begin to eject bodies. With gas, almost all mass is lost in ejections.

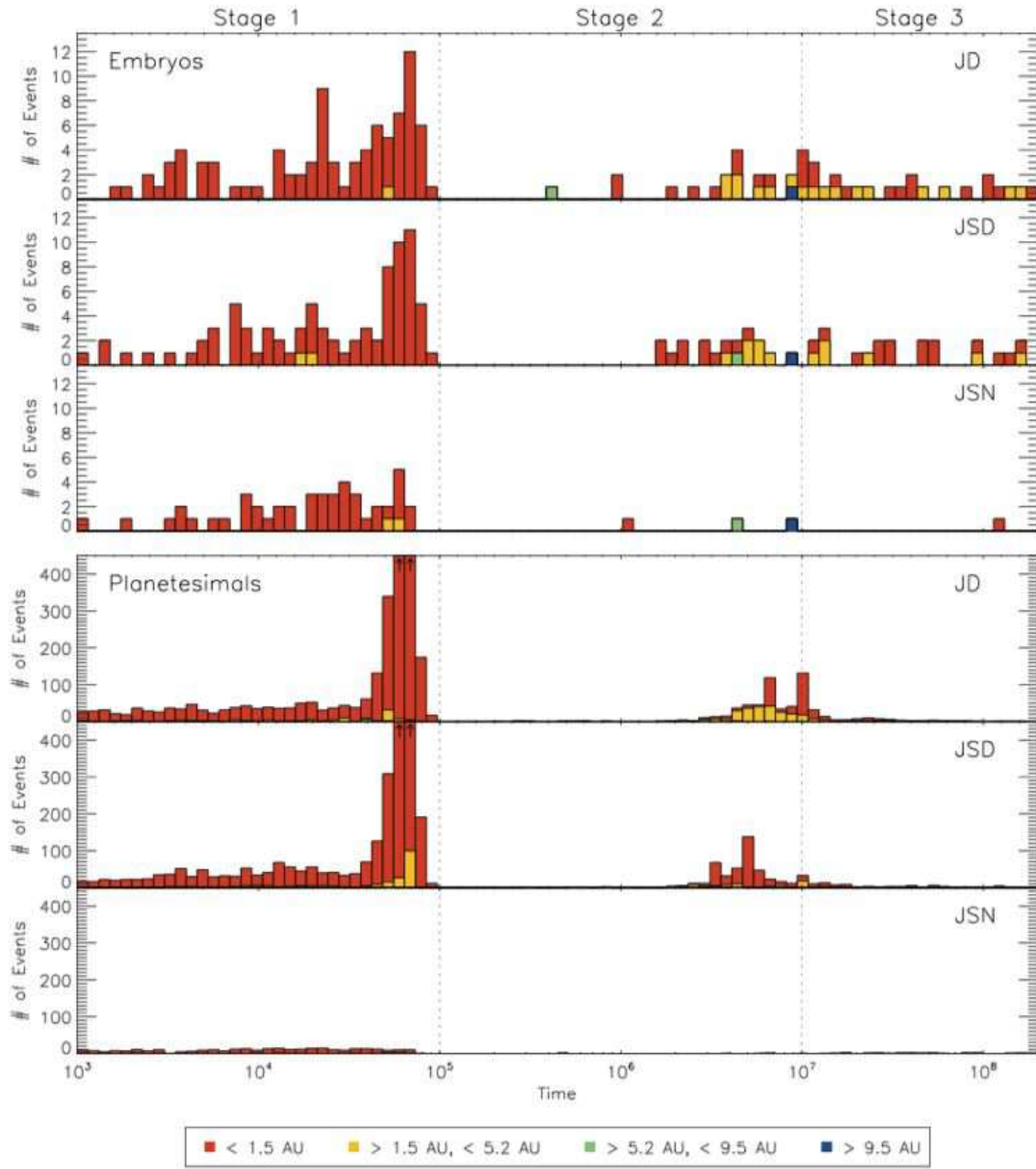


FIG. 7.— Number of bodies accreted as a function of time, with the radial location of the impact denoted by color, for the three different models. Accretion occurs almost solely within 1.5 AU during migration, with additional accretion occurring at a range of distances as the gas disk dissipates. Accretion is almost non-existent when the gas is dense enough to damp down orbital excitation.

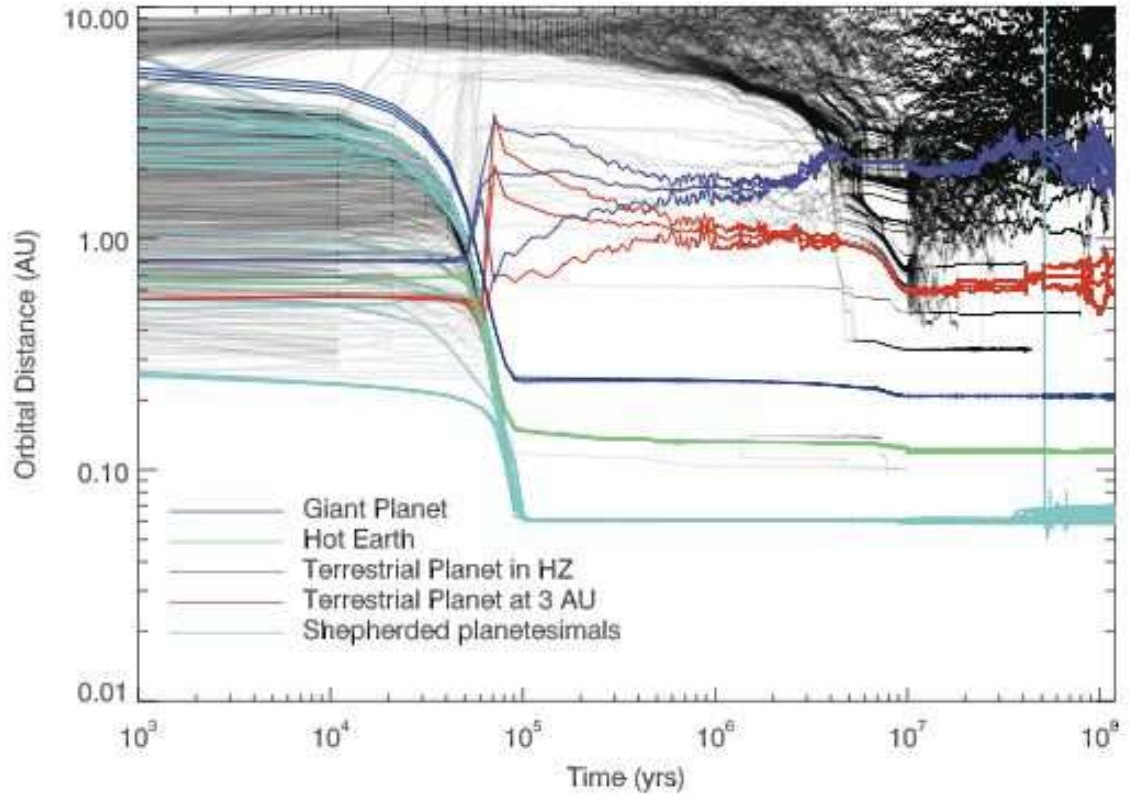


FIG. 8.— Plot of orbital distance with time for planetesimals (black) in a sample JD simulation. Colored lines denote the evolution of the initial accretion seeds for important bodies in the simulation. As the Jupiter-mass planet moves inward, planetesimals and embryos are shepherded in resonances to become 'hot Earths'. Other embryos are scattered outward to become outer terrestrial planets. Multiple lines show the range in orbital distance due to eccentricity.

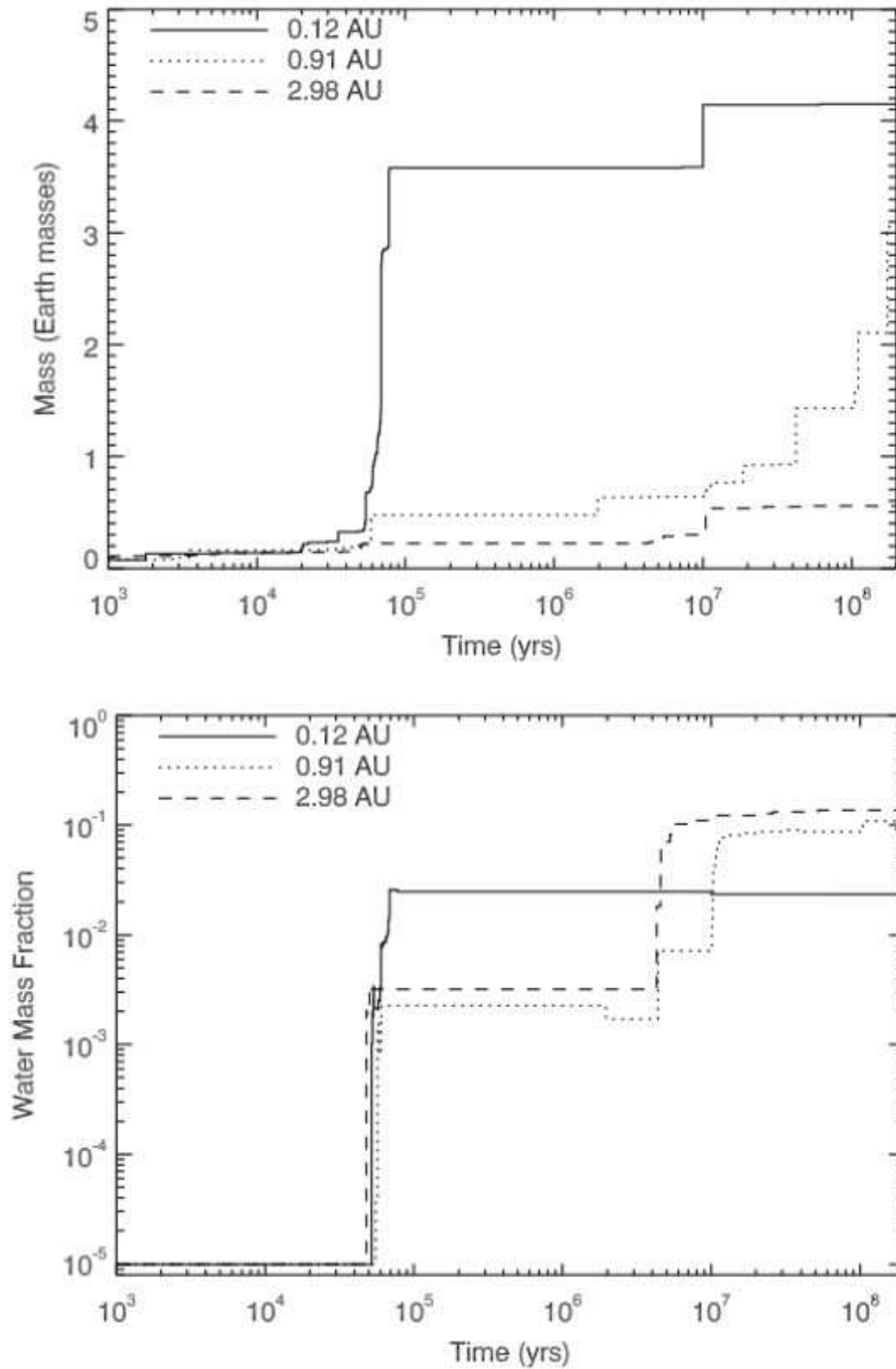


FIG. 9.— Plot of mass versus time (top) and water mass fraction versus time (bottom) for three indicative bodies in a sample JD simulation. The body that settles at 0.12 AU (a 'hot Earth') accretes very rapidly near the end of migration, while the outer terrestrial planets accrete material gradually over longer timescales. For the outer terrestrial planets, most of their water is accreted at two distinct times: just before scattering near the end of migration (Stage 1), and at the end of gas dissipation (Stage 2) when orbital excitation increases.

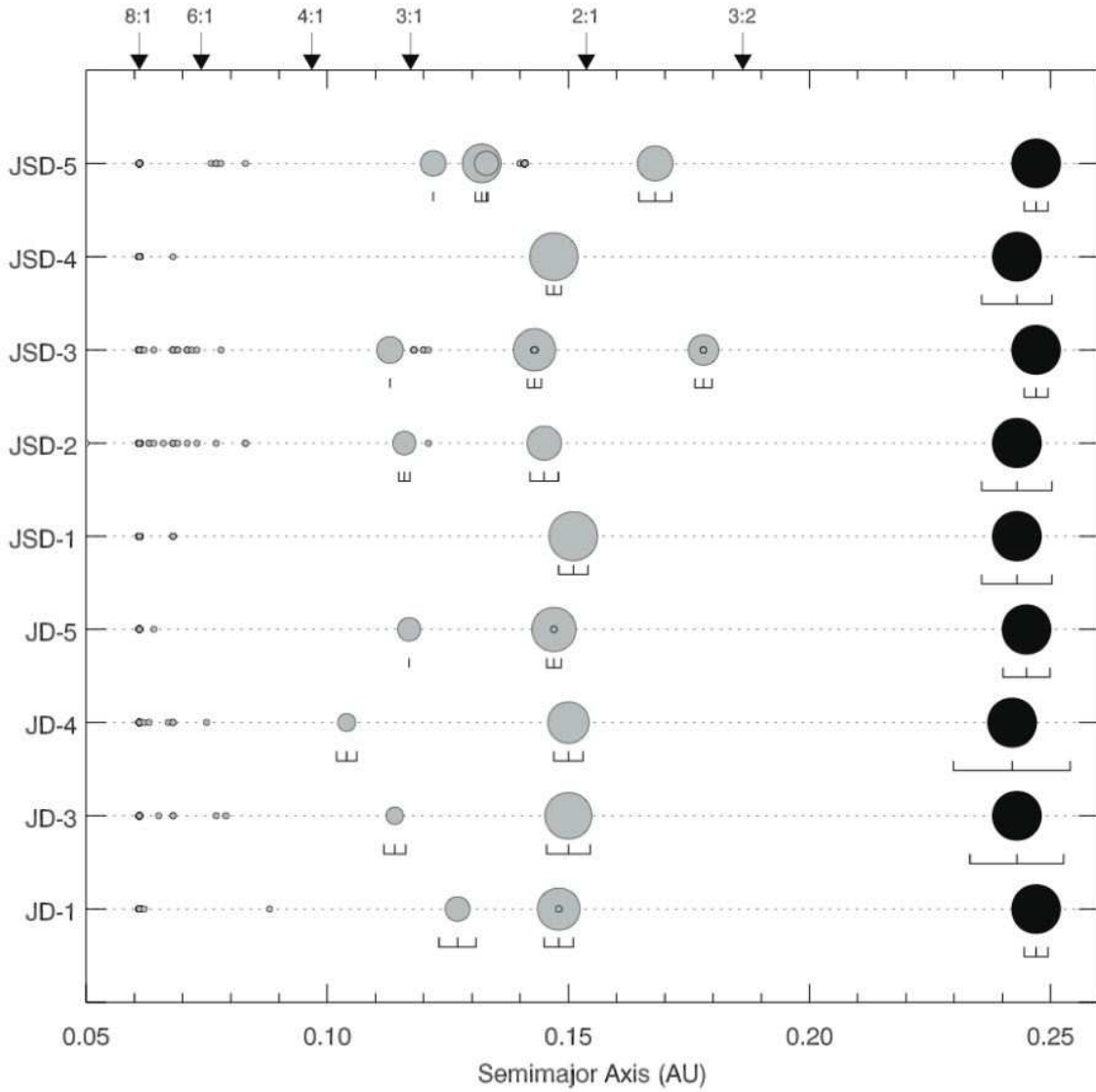


FIG. 10.— Final configurations for 'hot Earths' in all simulations with gas drag (JD and JSD) before instability sets in when the gas disk dissipates. Resonance positions for a 'hot Jupiter' at 0.25 AU are marked. The size of each body corresponds to its mass, with the orbital range (i.e. eccentricity) indicated below. It is clear that most 'hot Earths' reside just inside resonances, due to the combined shepherding effect of the resonance and the orbital decay from gas drag.

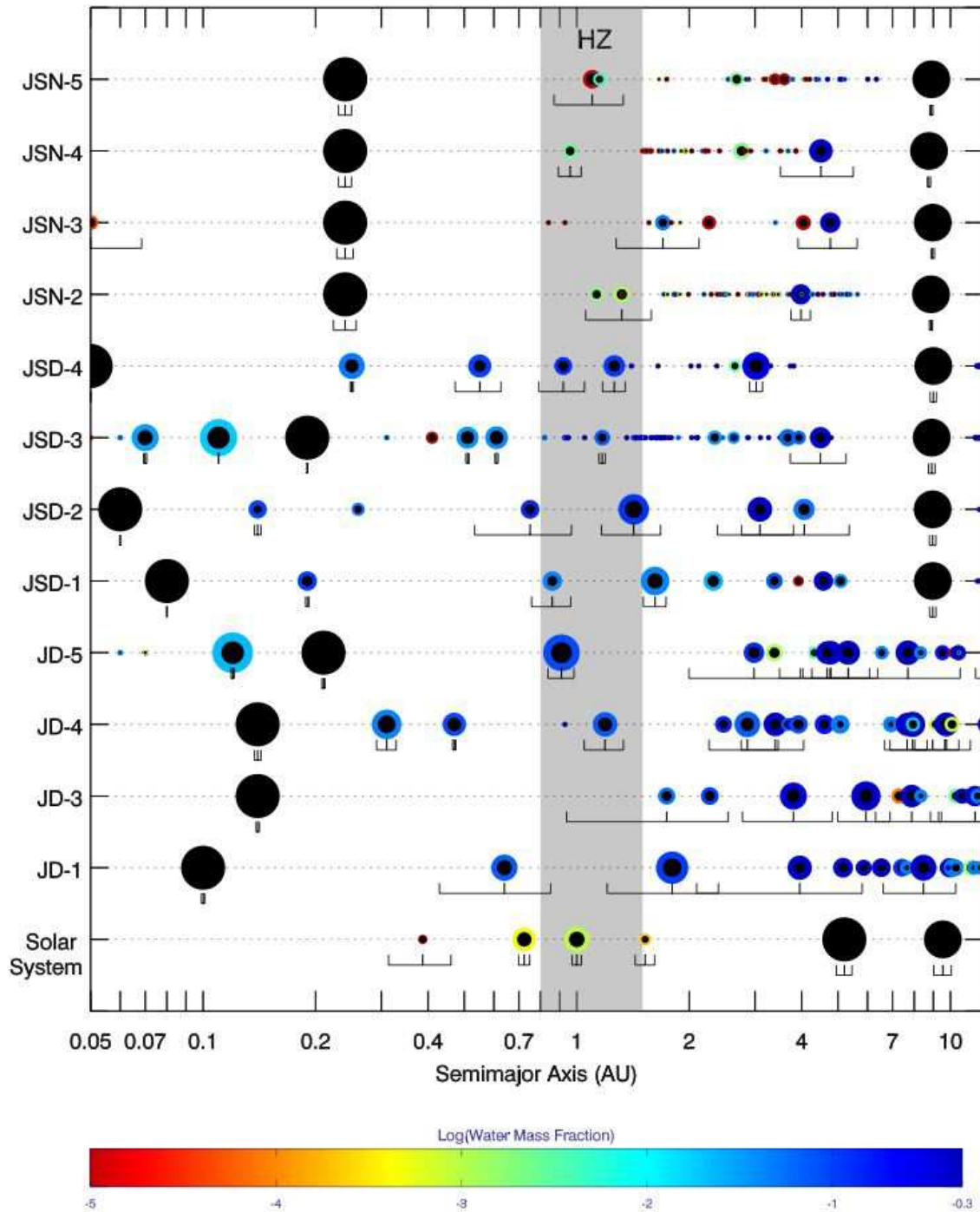


FIG. 11.— Final configurations for all the simulations after 200 Myr of integration. The size of each body indicates mass and the color indicates water content (with the Solar System plotted on the bottom for reference). The orbital range (i.e. eccentricity) for each body is indicated by the horizontal error-bar. It is clear that systems with long-lived gas disks will form more massive, water-rich planets in or near the Habitable Zone, but that planets will form even in systems without gas. Additionally, dense gas in the inner system will lead to 'hot Earths' near resonances with the 'hot Jupiter'.

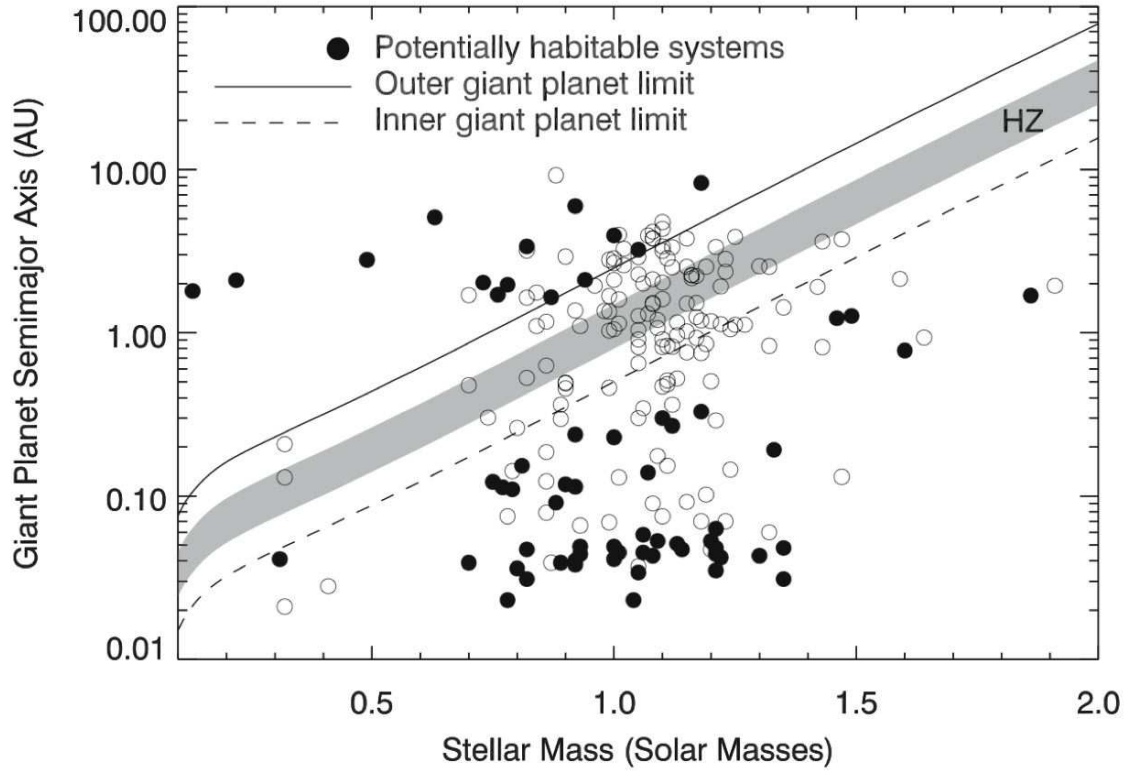


FIG. 12.— The known extrasolar planets that are likely to have formed terrestrial planets in the Habitable Zone. The solid line shows the outer giant planet semi-major axis limit for habitable planet formation from Raymond (2006), and the dashed line is the inner giant planet semi-major axis limit found from the current simulations. Filled circles indicate the known giant planets that satisfy our criteria (eccentricity less than 0.1 and semi-major axis within the derived limits) and may therefore harbor a terrestrial planet in the Habitable Zone; open circles are unlikely candidates for habitability. Note that not all planets above or below our limits qualify, due to the eccentricity limit. The Habitable Zone is shaded. Modified from Raymond et al. (2006b) (Paper I).

TABLE 1
EMBRYO/PLANETESIMAL PROPERTIES AT THE END OF STAGE 1

	Zone ¹	JD	JSD	JSN
Tot. Mass: Em/Pl	Z.1	7.60 M _⊕ / 0.31 M _⊕	7.97 M _⊕ / 0.53 M _⊕	1.90 M _⊕ / 1.43 M _⊕
	Z.2	6.18 M _⊕ / 1.42 M _⊕	3.24 M _⊕ / 0.70 M _⊕	4.18 M _⊕ / 1.37 M _⊕
	Z.3	2.77 M _⊕ / 0.07 M _⊕	4.93 M _⊕ / 0.50 M _⊕	3.36 M _⊕ / 1.79 M _⊕
Em. M (M _⊕) ²	Z.1	0.45 (0.07 – 4.35)	0.46 (0.08 – 4.90)	0.18 (0.05 – 0.54)
	Z.2	0.42 (0.08 – 1.23)	0.29 (0.09 – 1.10)	0.39 (0.05 – 1.05)
	Z.3	0.28 (0.09 – 0.88)	0.39 (0.10 – 1.10)	0.32 (0.03 – 1.23)
Em. log(W.M.F.) ²	Z.1	-2.09 (-5.00 – -1.26)	-1.74 (-5.00 – -0.30)	-1.75 (-5.00 – -0.30)
	Z.2	-0.56 (-5.00 – -0.30)	-0.72 (-5.00 – -0.30)	-0.59 (-5.00 – -0.30)
	Z.3	-0.85 (-5.00 – -0.30)	-0.60 (-5.00 – -0.30)	-0.75 (-5.00 – -0.30)
Em. log(Fe M.F.) ²	Z.1	-0.52 (-1.13 – -0.37)	-0.54 (-1.18 – -0.40)	-0.51 (-1.01 – -0.34)
	Z.2	-0.76 (-1.23 – -0.34)	-0.74 (-1.23 – -0.37)	-0.74 (-1.23 – -0.38)
	Z.3	-0.80 (-1.23 – -0.49)	-0.81 (-1.23 – -0.39)	-0.70 (-1.23 – -0.37)
Em. Eccen. ²	Z.1	0.44 (0.01 – 0.84)	0.48 (0.01 – 0.87)	0.61 (0.02 – 0.91)
	Z.2	0.37 (0.01 – 0.92)	0.42 (0.06 – 0.86)	0.44 (0.04 – 0.94)
	Z.3	0.75 (0.41 – 0.97)	0.62 (0.09 – 0.99)	0.71 (0.06 – 0.98)
Em. Incln.(°) ²	Z.1	6.62 (0.22 – 36.65)	8.49 (0.20 – 29.28)	26.34 (0.51 – 80.41)
	Z.2	5.25 (0.44 – 28.00)	12.89 (0.90 – 51.13)	19.79 (1.26 – 70.18)
	Z.3	4.69 (0.64 – 13.56)	11.79 (1.23 – 34.50)	17.09 (1.40 – 46.70)
Pl. Eccen. ²	Z.1	0.00 (0.00 – 0.10)	0.01 (0.00 – 0.19)	0.54 (0.06 – 0.94)
	Z.2	0.09 (0.00 – 0.23)	0.08 (0.01 – 0.40)	0.41 (0.01 – 0.97)
	Z.3	0.11 (0.01 – 0.21)	0.31 (0.02 – 0.79)	0.60 (0.02 – 0.99)
Pl. Incln.(°) ²	Z.1	0.08 (0.01 – 1.86)	0.50 (0.00 – 5.51)	28.65 (0.19 – 84.56)
	Z.2	2.58 (0.02 – 10.52)	3.67 (0.23 – 18.00)	17.93 (0.33 – 80.30)
	Z.3	2.36 (0.61 – 5.00)	5.69 (0.35 – 32.37)	14.94 (0.30 – 81.01)

¹ Radial zones are delineated as follows: Z.1 ($a < 5.2$ AU), Z.2 ($5.2 \leq a < 9.5$), and Z.3 ($9.5 \leq a$)

² Values represent the mean of the bodies in each zone, with the range of values in parentheses.

TABLE 2
EMBRYO/PLANETESIMAL PROPERTIES AT THE END OF STAGE 2

	Zone ¹	JD	JSD	JSN
Tot. Mass: Em/Pl	Z.1	9.25 M _⊕ / 1.01 M _⊕	5.77 M _⊕ / 0.51 M _⊕	1.34 M _⊕ / 0.82 M _⊕
	Z.2	5.12 M _⊕ / 0.02 M _⊕	0.63 M _⊕ / 0.01 M _⊕	0.67 M _⊕ / 0.19 M _⊕
	Z.3	2.65 M _⊕ / 0.00 M _⊕	0.26 M _⊕ / 0.44 M _⊕	1.04 M _⊕ / 0.24 M _⊕
Em. M (M _⊕) ²	Z.1	0.55 (0.09 – 4.59)	0.40 (0.08 – 4.44)	0.24 (0.11 – 0.81)
	Z.2	0.46 (0.12 – 1.59)	0.42 (0.14 – 0.95)	0.38 (0.14 – 0.60)
	Z.3	0.32 (0.11 – 0.93)	0.52 (0.15 – 0.90)	0.52 (0.12 – 1.05)
Em. log(W.M.F.) ²	Z.1	-1.03 (-5.00 – -0.30)	-1.03 (-5.00 – -0.30)	-1.26 (-5.00 – -0.30)
	Z.2	-0.54 (-4.41 – -0.30)	-0.57 (-2.74 – -0.30)	-0.53 (-5.00 – -0.30)
	Z.3	-0.72 (-5.00 – -0.30)	-0.56 (-1.30 – -0.30)	-0.50 (-5.00 – -0.30)
Em. log(Fe M.F.) ²	Z.1	-0.59 (-1.13 – -0.42)	-0.61 (-1.20 – -0.40)	-0.56 (-1.01 – -0.41)
	Z.2	-0.81 (-1.23 – -0.48)	-0.83 (-1.13 – -0.55)	-0.75 (-0.96 – -0.48)
	Z.3	-0.86 (-1.23 – -0.49)	-0.99 (-1.18 – -0.86)	-0.79 (-1.22 – -0.49)
Em. Eccen. ²	Z.1	0.13 (0.00 – 0.55)	0.07 (0.00 – 0.64)	0.34 (0.01 – 0.79)
	Z.2	0.29 (0.02 – 0.86)	0.17 (0.01 – 0.40)	0.40 (0.11 – 0.85)
	Z.3	0.53 (0.17 – 0.93)	0.73 (0.73 – 0.74)	0.42 (0.15 – 0.80)
Em. Incln.(°) ²	Z.1	2.63 (0.03 – 16.09)	2.07 (0.05 – 26.80)	20.87 (3.00 – 48.33)
	Z.2	6.85 (0.72 – 21.31)	5.53 (0.91 – 13.54)	32.45 (7.42 – 55.09)
	Z.3	6.77 (0.83 – 16.80)	21.40 (15.11 – 30.44)	22.97 (5.55 – 60.20)
Pl. Eccen. ²	Z.1	0.06 (0.00 – 0.31)	0.03 (0.00 – 0.31)	0.47 (0.04 – 0.85)
	Z.2	0.16 (0.05 – 0.25)	0.05 (0.02 – 0.11)	0.41 (0.03 – 0.92)
	Z.3	0.21 (0.18 – 0.23)	0.05 (0.00 – 0.29)	0.57 (0.06 – 0.97)
Pl. Incln.(°) ²	Z.1	1.48 (0.01 – 12.63)	1.18 (0.05 – 6.29)	27.68 (0.74 – 69.72)
	Z.2	8.03 (1.69 – 11.38)	1.73 (1.41 – 2.56)	27.78 (3.14 – 66.70)
	Z.3	6.54 (4.21 – 9.10)	1.82 (0.24 – 18.63)	27.09 (1.04 – 71.22)

¹ Radial zones are delineated as follows: Z.1 ($a < 5.2$ AU), Z.2 ($5.2 \leq a < 9.5$), and Z.3 ($9.5 \leq a$)

² Values represent the mean of the bodies in each zone, with the range of values in parentheses.

TABLE 3
FINAL EMBRYO/PLANETESIMAL PROPERTIES

	Zone ¹	JD	JSD	JSN
Tot. Mass: Em/Pl	Z.1	5.52 M _⊕ / 0.05 M _⊕	4.08 M _⊕ / 0.05 M _⊕	1.17 M _⊕ / 0.19 M _⊕
	Z.2	2.71 M _⊕ / 0.00 M _⊕	0.26 M _⊕ / 0.00 M _⊕	0.00 M _⊕ / 0.01 M _⊕
	Z.3	4.83 M _⊕ / 0.02 M _⊕	0.00 M _⊕ / 0.35 M _⊕	0.51 M _⊕ / 0.04 M _⊕
Em. M (M _⊕) ²	Z.1	1.03 (0.12 – 4.15)	0.58 (0.08 – 1.77)	0.29 (0.11 – 0.82)
	Z.2	0.48 (0.14 – 1.59)	0.35 (0.17 – 0.46)	0.00 (0.00 – 0.00)
	Z.3	0.32 (0.09 – 1.24)	0.00 (0.00 – 0.00)	1.03 (1.01 – 1.05)
Em. log(W.M.F.) ²	Z.1	-0.68 (-2.93 – -0.30)	-0.87 (-5.00 – -0.30)	-1.01 (-5.00 – -0.30)
	Z.2	-0.56 (-5.00 – -0.30)	-0.71 (-1.46 – -0.30)	0.00 (0.00 – 0.00)
	Z.3	-0.67 (-5.00 – -0.30)	0.00 (0.00 – 0.00)	-0.30 (-0.30 – -0.30)
Em. log(Fe M.F.) ²	Z.1	-0.65 (-0.96 – -0.50)	-0.65 (-1.19 – -0.44)	-0.55 (-0.94 – -0.42)
	Z.2	-0.81 (-1.21 – -0.54)	-0.69 (-0.88 – -0.59)	0.00 (0.00 – 0.00)
	Z.3	-0.81 (-1.23 – -0.48)	0.00 (0.00 – 0.00)	-0.91 (-0.93 – -0.90)
Em. Eccen. ²	Z.1	0.29 (0.01 – 0.74)	0.17 (0.00 – 0.57)	0.24 (0.03 – 0.42)
	Z.2	0.30 (0.08 – 0.58)	0.15 (0.12 – 0.35)	0.00 (0.00 – 0.00)
	Z.3	0.39 (0.06 – 0.95)	0.00 (0.00 – 0.00)	0.19 (0.13 – 0.24)
Em. Incln.(°) ²	Z.1	14.40 (0.69 – 32.24)	6.66 (0.35 – 21.80)	17.27 (3.71 – 28.34)
	Z.2	18.46 (4.73 – 42.86)	13.66 (6.50 – 19.22)	0.00 (0.00 – 0.00)
	Z.3	19.76 (2.71 – 50.25)	0.00 (0.00 – 0.00)	3.21 (2.74 – 3.82)
Pl. Eccen. ²	Z.1	0.13 (0.05 – 0.34)	0.44 (0.03 – 0.89)	0.40 (0.06 – 0.81)
	Z.2	0.67 (0.67 – 0.67)	0.37 (0.37 – 0.37)	0.43 (0.17 – 0.73)
	Z.3	0.69 (0.40 – 0.90)	0.08 (0.01 – 0.26)	0.28 (0.06 – 0.60)
Pl. Incln.(°) ²	Z.1	8.80 (2.28 – 50.79)	31.25 (2.02 – 61.23)	31.65 (2.02 – 59.38)
	Z.2	93.39 (93.39 – 93.39)	43.84 (43.84 – 43.84)	31.21 (8.42 – 48.70)
	Z.3	33.94 (12.39 – 92.93)	4.07 (0.21 – 27.00)	18.87 (4.03 – 42.56)

¹ Radial zones are delineated as follows: Z.1 ($a < 5.2$ AU), Z.2 ($5.2 \leq a < 9.5$), and Z.3 ($9.5 \leq a$)

² Values represent the mean of the bodies in each zone, with the range of values in parentheses.

TABLE 4
 PROPERTIES OF PLANETS FORMED IN JD SIMULATIONS¹

Simulation	$a(AU)$	\bar{e}^2	$\bar{i}(\circ)$	$M(M_{\oplus})$	W.M.F.	Fe M.F.
JD-1	0.10	0.01	0.6	323.42	—	—
	0.64	0.33	1.5	1.14	7.72×10^{-2}	0.27
	1.80	0.33	5.5	2.14	1.13×10^{-1}	0.27
	3.95	0.47	7.2	0.90	5.00×10^{-1}	0.11
	4.01	0.46	24.4	0.24	1.00×10^{-5}	0.29
JD-3	0.14	0.01	0.5	326.45	—	—
	1.74	0.46	38.0	0.32	5.78×10^{-2}	0.29
	2.27	0.48	22.9	0.36	1.01×10^{-1}	0.27
	3.80	0.27	9.0	1.25	4.05×10^{-1}	0.16
JD-4	0.14	0.02	0.3	324.17	—	—
	0.31	0.06	1.4	1.63	4.60×10^{-2}	0.31
	1.19	0.12	8.0	0.92	7.64×10^{-2}	0.27
	2.47	0.59	42.7	0.30	1.52×10^{-1}	0.24
	2.86	0.21	10.5	1.06	7.08×10^{-2}	0.20
	3.33	0.31	24.0	0.23	9.23×10^{-2}	0.28
	3.40	0.19	12.5	0.83	5.00×10^{-1}	0.11
	3.67	0.21	16.3	0.14	7.39×10^{-2}	0.26
	3.80	0.69	45.7	0.14	2.28×10^{-1}	0.22
	3.92	0.23	11.2	0.39	9.03×10^{-2}	0.26
4.60	0.32	10.3	0.46	1.79×10^{-1}	0.17	
JD-5	0.12	0.01	0.7	4.15	2.34×10^{-2}	0.25
	0.21	0.01	0.1	320.92	—	—
	0.91	0.08	5.0	3.05	9.23×10^{-2}	0.27
	2.98	0.33	13.3	0.55	1.36×10^{-1}	0.26
	3.38	0.22	11.9	0.32	1.15×10^{-3}	0.31
	4.32	0.51	27.7	0.12	3.77×10^{-3}	0.27
	4.78	0.27	14.9	0.84	5.00×10^{-1}	0.13
	4.68	0.14	13.5	0.72	5.00×10^{-1}	0.11

¹ Planets are defined to be $> 0.1 M_{\oplus}$ and inside 5 AU. Close-in giant planets are shown in bold.

² Orbital elements are averaged over the last Myr of the simulation.

TABLE 5
 PROPERTIES OF PLANETS FORMED IN JSD SIMULATIONS

Simulation	$a(AU)$	\bar{e}	$\bar{i}(^\circ)$	$M(M_\oplus)$	W.M.F.	Fe M.F.
JSD-1	0.08	0.00	0.2	325.57	—	—
	0.19	0.01	0.5	0.46	1.12×10^{-1}	0.25
	0.86	0.12	4.1	0.46	4.76×10^{-2}	0.20
	1.62	0.07	2.0	1.46	4.34×10^{-2}	0.23
	2.32	0.22	3.4	0.46	2.59×10^{-2}	0.30
	3.38	0.08	2.6	0.29	7.68×10^{-2}	0.23
	4.57	0.12	4.6	0.46	5.00×10^{-1}	0.13
JSD-2	0.06	0.00	2.3	325.67	—	—
	0.14	0.02	2.3	0.38	9.99×10^{-2}	0.13
	0.26	0.00	2.3	0.14	5.55×10^{-2}	0.28
	0.75	0.29	17.2	0.41	1.43×10^{-1}	0.23
	1.42	0.18	7.1	1.77	1.24×10^{-1}	0.27
	3.09	0.23	5.1	0.95	5.00×10^{-1}	0.12
	4.06	0.32	8.9	0.60	5.59×10^{-2}	0.23
JSD-3	0.07	0.01	0.7	1.24	3.25×10^{-2}	0.25
	0.11	0.00	0.6	3.23	1.92×10^{-2}	0.31
	0.19	0.00	0.6	320.21	—	—
	0.41	0.03	1.4	0.12	1.00×10^{-5}	0.35
	0.51	0.01	1.0	0.68	3.67×10^{-2}	0.32
	0.61	0.01	1.1	0.74	4.14×10^{-2}	0.32
	1.17	0.02	0.8	0.24	7.57×10^{-2}	0.23
	2.34	0.12	4.1	0.19	3.70×10^{-2}	0.28
	2.63	0.17	6.5	0.13	2.90×10^{-2}	0.31
	3.67	0.10	4.8	0.33	6.68×10^{-2}	0.16
	3.93	0.18	15.0	0.17	6.81×10^{-2}	0.20
	4.49	0.17	2.7	0.61	5.00×10^{-1}	0.12
JSD-4	0.05	0.00	2.1	324.82	—	—
	0.25	0.01	2.1	1.11	5.20×10^{-2}	0.20
	0.55	0.14	8.1	0.77	1.05×10^{-1}	0.19
	0.92	0.14	6.8	0.36	1.37×10^{-1}	0.27
	1.26	0.07	7.1	0.63	1.16×10^{-1}	0.21
	2.65	0.20	19.8	0.11	3.33×10^{-3}	0.27
	3.02	0.04	2.0	1.32	3.25×10^{-1}	0.17

TABLE 6
 PROPERTIES OF PLANETS FORMED IN JSN SIMULATIONS

Simulation	$a(AU)$	\bar{e}	$\bar{i}(^\circ)$	$M(M_\oplus)$	W.M.F.	Fe M.F.
JSN-2	0.24	0.07	1.1	318.85	—	—
	1.13	0.35	24.9	0.19	1.84×10^{-3}	0.30
	1.32	0.20	17.0	0.28	1.26×10^{-3}	0.35
	3.98	0.06	10.2	0.53	4.93×10^{-1}	0.13
JSN-3	0.05	0.37	29.3	0.22	4.99×10^{-1}	0.11
	0.24	0.05	3.7	318.82	—	—
	1.70	0.25	3.8	0.24	4.85×10^{-2}	0.24
	2.26	0.04	7.0	0.18	1×10^{-5}	0.30
	4.04	0.40	21.2	0.22	1×10^{-5}	0.29
	4.77	0.18	14.0	0.54	5.00×10^{-1}	0.14
	22.70	0.25	3.8	1.01	5.00×10^{-1}	0.12
JSN-4	0.24	0.04	1.7	319.29	—	—
	0.96	0.07	17.3	0.22	2.46×10^{-3}	0.28
	2.76	0.04	28.9	0.30	2.13×10^{-3}	0.26
	4.50	0.22	12.4	0.82	5.00×10^{-1}	0.11
	18.53	0.13	3.6	1.05	5.00×10^{-1}	0.13
JSN-5	0.24	0.04	2.0	319.10	—	—
	1.10	0.21	12.0	0.40	1×10^{-5}	0.36
	1.15	0.31	24.6	0.13	5.44×10^{-3}	0.29
	2.68	0.28	13.3	0.17	2.02×10^{-3}	0.38
	3.39	0.47	23.4	0.11	1×10^{-5}	0.31
	3.59	0.24	20.0	0.12	1×10^{-5}	0.32

TABLE 7
GIANT PLANET SEMI-MAJOR AXIS LIMITS FOR POTENTIALLY HABITABLE SYSTEMS

M_* (M_\odot)	Sp. Type ¹	Hab Zone (AU) ²	Inner Limit (AU)	Outer Limit (AU)
0.1	M6	0.024 - 0.045	0.015	0.075
0.4	M3	0.10 - 0.19	0.06	0.32
0.7	K6	0.28 - 0.52	0.17	0.87
1.0	G2	0.8 - 1.5	0.5	2.5
1.3	F8	2.3 - 4.3	1.45	7.2
1.6	F0	6.5 - 12.3	4.1	20.5
2.0	A5	25 - 47	15.7	78.3

¹ Spectral types from Table 8.1 of Reid & Hawley (2000) and Appendix E from Carroll & Ostlie (1996). Spectral types of low-mass stars are age-dependent.

² Habitable Zones scaled by $L_*^{1/2}$ to 0.8 - 1.5 AU for a solar-mass star.

TABLE 8
POTENTIALLY HABITABLE EXOPLANET SYSTEMS¹

System	M_{\star} (M_{\odot})	[Fe/H]	M_{pl} (M_J)	a (AU)	e	HZ
OGLE-05-071L	0.13	—	0.9	1.800	—	0.03-0.06
OGLE-05-390L	0.22	—	0.02	2.100	—	0.06-0.10
GJ 581	0.31	-0.25	0.052	0.041	0.00	0.08-0.14
OGLE235-MOA53	0.36	—	1.5	3.000	—	0.09-0.17
HD 41004 A	0.40	0.16	17.892	0.018	0.08	0.10-0.19
OGLE-05-169L	0.49	—	0.04	2.800	—	0.14-0.25
HD 330075	0.70	0.08	0.623	0.039	0.00	0.28-0.52
HD 27894	0.75	0.3	0.618	0.122	0.05	0.33-0.62
HD 114386	0.76	0.004	1.343	1.714	0.23	0.34-0.64
HD 13445	0.77	-0.27	3.9	0.113	0.04	0.35-0.66
OGLE-TR-113	0.77	0.14	1.35	0.023	0.00	0.35-0.66
HD 111232	0.78	-0.36	6.803	1.975	0.20	0.37-0.69
HD 63454	0.80	0.11	0.385	0.036	0.00	0.39-0.74
HD 192263	0.81	0.05	0.641	0.153	0.05	0.41-0.76
OGLE-TR-111	0.81	0.12	0.52	0.047	0.00	0.41-0.76
Eps Eri	0.82	-0.03	1.058	3.377	0.25	0.42-0.79
HD 189733	0.82	-0.03	1.152	0.031	0.00	0.42-0.79
HD 130322	0.88	0.006	1.088	0.091	0.02	0.52-0.98
TrES-1	0.89	0.001	0.759	0.039	0.00	0.54-1.01
HD 4308	0.90	-0.31	0.047	0.118	0.00	0.56-1.05
55 Cnc e	0.91	0.31	0.038	0.038	0.09	0.58-1.09
55 Cnc b			0.833	0.114	0.01	0.58-1.09
55 Cnc c			0.157	0.238	0.07	0.58-1.09
55 Cnc d			3.887	5.964	0.09	0.58-1.09
HD 46375	0.92	0.24	0.226	0.040	0.06	0.60-1.13
HD 2638	0.93	0.16	0.477	0.044	0.00	0.62-1.17
HD 102195	0.93	-0.09	0.492	0.049	0.06	0.62-1.17
HD 164922	0.94	0.17	0.36	2.110	0.05	0.65-1.21
HD 89307	1.00	-0.16	2.601	3.945	0.01	0.80-1.50
HD 83443	1.00	0.36	0.398	0.041	0.01	0.80-1.50
Rho Cnc B	1.00	-0.20	1.092	0.229	0.06	0.80-1.50
BD -10 3166	1.01	0.38	0.458	0.045	0.02	0.83-1.55
HD 70642	1.05	0.16	1.97	3.230	0.03	0.96-1.79
HD 73256	1.05	0.26	1.867	0.037	0.03	0.96-1.79
HD 212301	1.05	-0.18	0.396	0.034	0.00	0.96-1.79
HD 49674	1.06	0.31	0.105	0.058	0.09	0.99-1.86
HD 195019	1.07	0.07	3.681	0.139	0.01	1.03-1.92
HD 187123	1.08	0.12	0.527	0.043	0.02	1.06-1.99
51 Peg	1.09	0.20	0.472	0.053	0.01	1.10-2.07
HD 107148	1.12	0.31	0.21	0.269	0.05	1.23-2.30
HD 76700	1.13	0.35	0.232	0.051	0.09	1.27-2.38
HD 209458	1.14	0.014	0.689	0.047	0.00	1.31-2.47
OGLE-TR-10	1.17	0.12	0.63	0.042	0.00	1.46-2.74
OGLE-TR-56	1.17	—	1.24	0.023	—	1.46-2.74
HD 121504	1.18	0.16	1.221	0.329	0.03	1.51-2.84
HD 149143	1.20	0.25	1.327	0.053	0.00	1.63-3.05
HD 75289	1.21	0.22	0.466	0.048	0.03	1.68-3.16
HD 109749	1.21	0.26	0.277	0.063	0.00	1.68-3.16
HD 179949	1.21	0.14	0.916	0.044	0.02	1.68-3.16
HD 86081	1.21	0.26	1.49	0.035	0.01	1.68-3.16
HD 149026	1.30	0.36	0.337	0.043	0.00	2.31-4.34
HD 224693	1.33	0.34	0.718	0.192	0.04	2.57-4.82
Tau Boo	1.35	0.23	4.126	0.048	0.02	2.76-5.17
OGLE-TR-132	1.35	0.43	1.19	0.031	0.00	2.76-5.17
HD 177830	1.46	0.54	1.531	1.227	0.10	4.04-7.58
Eps Ret	1.49	0.42	1.556	1.270	0.06	4.48-8.41
HD 104985	1.60	-0.35	6.315	0.779	0.03	6.55-12.27

¹ Data from Butler et al (2006), www.exoplanet.eu, and references therein.